Astron. Astrophys. 329, 639–658 (1998)

ASTRONOMY AND ASTROPHYSICS

Constraints on cosmic-ray origin from TeV gamma-ray observations of supernova remnants

J.H. Buckley[1], C.W. Akerlof[2], D.A. Carter-Lewis[3], M. Catanese[3], M.F. Cawley[4], V. Connaughton[5], D.J. Fegan[6], J.P. Finley[7], J.A. Gaidos[7], A.M. Hillas[8], F. Krennrich[3], R.C. Lamb[9,3], R.W. Lessard[7], J.E. McEnery[6], G. Mohanty[3], J. Quinn[10,6], A.J. Rodgers[8], H.J. Rose[8], A.C. Rovero[11], M.S. Schubnell[2], G. Sembroski[7], R. Srinivasan[7], T.C. Weekes[10], and J. Zweerink[3]

[1] Department of Physics, Washington University, St. Louis, MD 63130, USA
[2] Randall Laboratory of Physics, University of Michigan, Ann Arbor, MI 48109-1120, USA
[3] Department of Physics and Astronomy, Iowa State University, Ames, IA 50011-3160, USA
[4] Physics Department, St.Patrick's College, Maynooth, Ireland
[5] NASA Marshall Space Flight Center, Huntsville, AL 35812, USA
[6] Physics Department, University College, Dublin 4, Ireland
[7] Department of Physics, Purdue University, West Lafayette, IN 47907, USA
[8] Physics Department, University of Leeds, Leeds, LS2 9JT, Yorkshire, UK
[9] Space Radiation Laboratory, California Institute of Technology, Pasadena, CA 91125, USA
[10] Whipple Observatory, Harvard-Smithsonian CfA, P.O. Box 97, Amado AZ 85645-0097, USA
[11] Insituto de Astronomía y Físca del Espacio, CC 67, Suc. 28, (1428) Buenos Aires, Argentina

Received 5 June 1997 / Accepted 21 July 1997

Abstract. If supernova remnants (SNRs) are the site of cosmic-ray acceleration, the associated nuclear interactions should result in an observable flux of γ-rays for the nearest SNRs. Measurements of the TeV γ-ray flux from six nearby, radio-bright SNRs have been made with the Whipple Observatory imaging air Čerenkov telescope over the period September 1993 to June 1996. No significant emission has been detected and upper limits on the >300 GeV flux are reported. Three of these SNRs (IC443, γ-Cygni and W44) are spatially coincident with low-latitude otherwise unidentified sources detected with the *Energetic Gamma-Ray Experiment Telescope* (EGRET). If the EGRET γ-ray fluxes result from cosmic-ray interactions then the EGRET and Whipple data are found to be collectively inconsistent with a cosmic-ray source spectrum flatter than $\sim E^{-2.4}$. The Whipple upper limits for IC443 and γ-Cygni are also inconsistent with a priori predictions if these remnants are indeed expanding into regions where the average density of the interstellar medium is enhanced by the presence of molecular clouds. These data weaken the case for the simplest models of shock acceleration and energy dependent propagation of cosmic rays.

Key words: gamma-rays: observations – SNRs – cosmic rays – ISM: IC 443; γ Cyg SNR; W 44

Send offprint requests to: J.H. Buckley

1. Introduction

It is now generally believed that cosmic rays with energies less than ∼100 TeV originate in the galaxy and are accelerated in shock waves in shell-type supernova remnants. Supernova blast shocks are one of the few galactic sites capable of satisfying the power budget of the galactic cosmic rays, although a high efficiency, ∼10%-30% (e.g., Drury et al. 1989), for converting the kinetic energy of the SNR explosions is required. The model of diffusive shock acceleration (e.g., Axford et al. 1977; Krymsky 1977; Blandford & Ostriker 1978; Bell 1978; Legage & Cesarsky 1983) provides a plausible mechanism for efficiently converting this explosion energy into accelerated particles with energies up to $\sim 10^{14} - 10^{15}$ eV (e.g., Völk 1987) and naturally gives a power-law spectrum similar to that inferred from the cosmic-ray data after correcting for the effects of propagation in the galaxy (e.g., Swordy et al. 1990). However plausible the theoretical arguments, the observational data are inconclusive and the question of the origin of cosmic-ray nuclei remains open.

The case for shock acceleration of electrons in SNRs is supported by the observations of radio and possibly X-ray synchrotron emission in SNR shells. Although in some objects the enhanced synchrotron emission could be due to ambient electrons interacting with the compressed magnetic fields at the shock front (van der Laan 1962), the synchrotron spectrum in many of these objects indicates electrons with a spectrum $\sim E^{-2}$, consistent with the predictions of shock acceleration (Reynolds & Ellison 1992; Reynolds 1995). Significantly, a re-

cent observation of the SNR SN1006 with the *Advanced Satellite for Cosmology and Astrophysics (ASCA)* shows evidence for nonthermal X-ray emission in the limbs of the remnant (Koyama et al. 1995). Reynolds (1996) has interpreted this X-ray data as synchrotron emission from nonthermal electrons accelerated to $\sim$100 TeV by the SNR shock. Observations of hard X-ray emission coincident with the shell of the supernova remnant IC443 have also been interpreted as giving evidence for local shock acceleration of electrons to energies of $\sim$20 TeV (Keohane et al. 1997). These electrons must be accelerated in situ since, at this energy, they could not have traversed far from their origin without suffering significant synchrotron losses. There is also indisputable evidence for the acceleration of electrons by a very different mechanism in the pulsar-powered (plerionic) SNRs. It is difficult to extrapolate from these data to any inferences about the acceleration of nucleons in these same objects.

If SNRs are indeed the source of the galactic cosmic rays, then they should also be sources of π_0-decay γ-rays produced as the cosmic rays interact with ambient matter in the vicinity of supernova shells. Our expectations for the γ-ray signal from SNRs are closely tied to experimental data, including direct measurements of the cosmic-ray spectra and the cosmic-ray energy density. The primary cosmic-ray nuclei (H, He, C, O, Fe) are all observed to have power law spectra approximately proportional to $E^{-2.7\pm0.1}$ up to at least TeV energies (e.g., Swordy et al. 1990; Buckley et al. 1994). The observed energy dependence in the ratio of secondary (spallation-produced) nuclei to these primary nuclei is most naturally explained if the propagation pathlength λ (which measures the total amount of material traversed within the propagation time) decreases with energy according to $\lambda \sim E^{-\delta}$. A value of $\delta \approx 0.6$ is derived from data taken with the HEAO3-C2 and CRN experiments (Engelmann et al. 1990; Swordy et al. 1990.) If propagation effects have steepened the spectra of secondary nuclei by E^{δ} with respect to that of their parent primary nuclei, then the observed spectra of primary nuclei $\sim E^{-2.7}$ should also be steepened by this power with respect to the source cosmic-ray spectrum. This leads to the inference that the differential cosmic ray spectrum is $\sim E^{-2.1\pm0.1}$ *at the source*. In the context of this model, the power budget for cosmic rays (derived from the observed supernova rate, the cosmic-ray energy density, and the cosmic-ray confinement time) is raised and on average 10-30% of the 10^{51} erg of kinetic energy for each supernova explosion must be converted into cosmic rays (e.g., Drury et al. 1989). Combining these constraints on the source cosmic ray flux with the measured values for the ambient density around each SNR one obtains a prediction for the γ-ray luminosity which is insensitive to many of the details of the acceleration mechanism.

Implicit in these arguments are the assumptions that the cosmic rays are in fact of galactic origin and are produced by a single mechanism from GeV to TeV energies. These assumptions are strongly supported by experimental data. A recent observation by EGRET provides evidence that cosmic rays at GeV energies are galactic: the upper limit on high energy γ-ray emission from the small Magellanic cloud (Sreekumar et al. 1993) lies significantly below the predicted flux from nuclear interactions between a universal extragalactic flux of cosmic rays and material in the SMC. The continuity of the spectra for the individual nuclear species, as well as that of the combined all-particle spectrum up to $\sim 10^{14} - 10^{15}$ eV, argues strongly that a single galactic mechanism accounts for the cosmic rays between 1 GeV and 10^{14} eV.

Drury, Aharonian & Völk (1994 [DAV]) and Naito & Takahara (1994) have calculated the expected γ-ray flux from secondary pion production using the model of diffusive shock acceleration. While an additional contribution from Inverse Compton scattering of ambient photons by either primary or secondary electrons (Mastichiadis 1996) or from high energy electron bremsstrahlung may also be present, these calculations give a lower limit on the predicted γ-ray flux. They predict that the cosmic-ray density and hence the associated γ-ray luminosity will increase with time as the SNR passes through its free expansion phase, will peak when the SNR enters its Sedov phase (i.e., the mass of swept-up material is equal to the mass of the ejecta) and level off throughout the Sedov phase and gradually decline thereafter. In order that the mechanism of diffusive shock acceleration be viable, the shock must be able to continuously overtake the diffusing cosmic rays which eventually escape downstream inside the SNR shell. Thus the enhanced cosmic-ray density and γ-ray emission should appear either near the shell or within the remnant.

For example, following DAV a SNR at a distance of 2 kpc, with an ambient density of 1 cm^{-3}, the canonical explosion energy $\approx 10^{51}$ ergs and an efficiency of $\theta = 0.15$ for converting this energy to cosmic rays, should have a luminosity of 160 mCrab at TeV energies, implying that such an object could be detected by the Whipple Observatory 10m γ-ray telescope. However, due to the angular extent of these objects, the sensitivity of the imaging Čerenkov technique is reduced and SNRs with special conditions (e.g., high ISM densities) must be selected for observations.

Here we report on the results of observations of six SNRs (IC443, γ-Cygni, W44, W51, W63 and Tycho) made over the period 1993-1996. These were selected on the basis of the following criteria: the SNR is (1) radio bright (> 50 Jy), thus showing evidence for nonthermal emission from electrons; (2) classified as a shell-type or composite remnant (shell-type radio and filled X-ray) (Green 1995); (3) relatively nearby ($\lesssim 3$ kpc), (4) old enough to be close to its Sedov phase; (5) of small angular size ($< 1^\circ$); and (6) possibly associated with a molecular cloud. For at least three of these SNRs (γ-Cygni, W44 and IC443) there is a clear association with a nearby unidentified EGRET source (Esposito et al. 1996). For a number of other unidentified sources there is also a suggestion of a correlation with a SNR (Sturner & Dermer 1994; Esposito et al. 1996). While Esposito et al. (1996) argue that these results suggest that supernova remnants are the acceleration sites of galactic cosmic rays, alternate explanations for the emission from these objects include emission from the pulsar B1853+01 for W44 (De Jager & Mastichiadis 1997), and emission from a previously unidentified radio-quiet pulsar for the γ-Cygni remnant (Brazier et al. 1996). In general the EGRET measurements are complicated

by uncertainties in the high level of diffuse background in the galactic plane (e.g., Mattox et al. 1996). At TeV energies the diffuse background ($\sim E^{-2.7}$) is greatly suppressed relative to the expected γ-ray signal, and the good angular resolution of the Whipple Observatory telescope $\sigma \approx 0.^\circ13$ should make it possible to distinguish between extended and point sources.

In §2 we describe the Whipple γ-ray telescope and describe the selection of candidate SNRs based on their predicted γ-ray luminosity. A new technique developed for analysis of emission from extended sources is presented in §3. In §4 we present our results in the form of two dimensional maps of the γ-ray emission over a 3° region surrounding the remnants as well as quantitative upper limits on the emission from the remnant taken as a whole. In §5 these upper limits are compared with an extrapolation of the EGRET results as well as detailed predictions of the γ-ray flux derived from the properties of each SNR.

2. Observations

2.1. The Whipple γ-ray telescope

The high-energy γ-ray telescope (Cawley et al. 1990) at the Whipple Observatory employs a 10 m diameter optical reflector to image Čerenkov light from air showers onto an array of 109 fast photomultipliers covering a 3° field of view. By making use of the distinctive differences in the angular distribution of light and orientation of the shower images, a γ-ray signal can be extracted from the large background of hadronic showers. Using this technique, a background rejection power of several hundred can be obtained. Monte Carlo simulations have shown that this analysis results in an effective energy threshold of approximately 300 GeV and an effective area of $\approx 3.5 \times 10^8 \mathrm{cm}^2$.

2.2. Predicted γ-ray fluxes from candidate sources

DAV derive the integral γ-ray flux from secondary π^0-decay resulting from interactions of cosmic-ray protons with the interstellar medium:

$$F_\gamma(\geq E) = f_\alpha \times 10^{-10} \mathscr{A} \left(\frac{E}{1\ \mathrm{TeV}}\right)^{-\alpha+1} \mathrm{cm}^{-2}\mathrm{s}^{-1} \qquad (1)$$

$$\mathscr{A} = \theta \left(\frac{E_{\mathrm{SN}}}{10^{51}\mathrm{erg}}\right) \left(\frac{d}{1\ \mathrm{kpc}}\right)^{-2} \left(\frac{n}{1\ \mathrm{cm}^{-3}}\right)$$

where $\mathscr{A}$ is a dimensionless scaling factor which includes the unique properties of the SNR including n the volume-averaged ambient hydrogen density, d the distance to the source and E_{SN} the kinetic energy of the explosion. The fraction of the explosion energy which is converted into cosmic-ray energy is given by the efficiency factor θ and $f_\alpha \approx 0.9$, 0.43, and 0.19 for a source spectral index of α=2.1, 2.2 and 2.3 respectively.

Our selection criteria require that candidate sources be nearby (within a few kpc), show evidence for strong nonthermal radio emission concentrated in a radio shell, have entered their Sedov phase, and be expanding into regions of enhanced hydrogen density. Properties of the selected remnants are summarized in Table 1. Here we consider the properties of the candidate SNRs, and estimate the reasonable range of values for the quantity $\mathscr{A}$.

The radio brightness and spectrum give an indication of the presence of nonthermal electrons and provide indirect evidence for the local acceleration of cosmic-ray nuclei. The synchrotron spectrum $\nu^{-\alpha}$ is related to the differential electron spectrum $\propto E^{-q}$ according to the relation $\alpha = (q-1)/2$. Synchrotron spectra with $\alpha = 0.5$ indicate electrons with a spectrum $\sim E^{-2}$ consistent with the predictions of shock acceleration. If nonlinear effects on the shock structure are taken into account, the effective compression ratio for electrons may be somewhat reduced resulting in a softer spectrum with $\alpha = 0.5 - 0.7$ (Ellison & Reynolds 1991; Reynolds & Ellison 1992).

The radio and X-ray morphology are also important to the selection of the remnant. While all of these objects show a clear radio-shell structure, most of the SNRs on our list also have a centrally peaked X-ray morphology which defines the class of composite remnants (Tycho is the exception). It is tempting to associate this emission with the synchrotron nebula around a pulsar, but with the possible exception of W44 (Harrus et al. 1996) none of these remnants show evidence for a Crab-like (plerionic) X-ray synchrotron component, and only W44 has a clearly associated radio pulsar. Alternate explanations for the centrally peaked morphology include: interaction of the shock with a pre-existing stellar wind bubble, presence of a reverse shock, interaction with or obscuration by molecular clouds, evaporation of shocked clouds, or radiation from the low density hot interior left as a remnant ages (e.g., Rho 1995).

The parameters E_{SN} and n, which are critical to making quantitative predictions of the γ-ray flux from cosmic-ray interactions are often provided by radio and X-ray observations. Following Esposito et al. (1996), the number density can also be derived from the three-dimensional matter distribution in the galaxy as inferred by Bertsch et al. (1993) from molecular cloud surveys, galactic rotation curves and the diffuse γ-ray data. From the diffuse γ-ray data it is unlikely that the density is much less than $n \approx 1\ \mathrm{cm}^{-3}$ for objects near the galactic plane. Except for a relatively small number of objects the exact values of these parameters are quite uncertain. E_{SN} is commonly assumed to be equal to the canonical value 10^{51}erg. Type Ia supernovae (probably the thermonuclear explosion of a white dwarf initiated by accretion from a companion star) are expected to release a constant amount of energy near this value, but it is unclear what fraction of the total energy ($\sim 10^{53}$ erg) is converted into kinetic energy for type II and type Ib supernovae (formed by core collapse of young massive stars) (Drury 1995).

X-ray observations have provided the morphology, brightness, and temperature, T, of the hot gas in the shells of most known galactic remnants. From these the density of the hot gas, n, can be calculated. A blast-wave model, fitted to the observations, can give a reasonable estimate of E_{SN} (e.g., Seward et al. 1996). Since it is the density of the hot inter-cloud gas which is typically derived from the X-ray data, this should be taken as a lower limit on the average density which must also include the

cloud component. In addition to the large uncertainty in the density of the ISM, distances to SNRs are notoriously unreliable, frequently varying by factors of $\sim$2 or more for many objects. However, a combination of kinematic distances, the placing of remnants with respect to molecular clouds, and measurement of X-ray absorption can reduce uncertainties.

For each remnant we give a brief survey of the derived values for the critical parameters E_{SN}, n and d in the following sections. Since the inferred values of n and E_{SN} depend on the distance, in calculating $\mathscr{A}$ we take together consistent sets of values for d, n and E_{SN} derived in different analyses. We also verify that the age and other dynamical properties of the remnant are consistent with it being in its Sedov phase, giving time for cosmic-ray acceleration to have taken place. We also consider evidence for spatial associations of SNRs with molecular clouds (for γ-Cygni and W63) as well as direct evidence of shocked cloud material for some of these remnants (IC443, W44 and W51), since the high density of such clouds (typically $\sim$ 200 cm^{-3}) can lead to a greatly enhanced γ-ray signal. Finally, the evidence for γ-ray emission at $>$ 100 MeV is considered for each candidate SNR.

2.3. G78.2 + 2.1 (the γ Cygni SNR)

This SNR has historically drawn the most attention based on its association with the strong COS-B source 2CG78+01 (Pollock 1985) and with the EGRET unidentified source, 2EG 2020+4026. The possibility that the SNR shock has overtaken a dense molecular cloud has also made this an attractive candidate for γ-ray observations (Aharonian, Drury & Völk 1995 [ADV]). The EGRET flux is $12.6\pm0.7\times10^{-7}$photons cm^{-2}s^{-1} and a flat spectrum of α = 2.07$\pm$0.05 has been derived for the source (Esposito et al. 1996). Esposito et al. (1996) interpret these results as being consistent with the predicted γ-ray emission resulting from nuclear interactions of cosmic-rays accelerated in the remnant. However, Brazier et al. (1996) have analyzed the 1 GeV data and have determined that the emission is not consistent with the spatial extent of the remnant, and offer an alternative association with the ROSAT source RX J2020.2+4026. This identification is still unclear, however, since the X-ray source is close to a star which could emit the observed X-ray flux but for which no γ-ray emission would be expected (Brazier et al. 1996).

G78.2+2.1 is a large radio shell-type remnant (see contours of the nonthermal component shown in Fig. 3b) of approximately 60′ diameter with a nonthermal radio spectrum of index α = $-$0.65 (Higgs et al. 1977) and a very high 1 GHz radio flux of 340 Jy (Green 1995). The radio-bright region DR4 in the southeast portion of the remnant is thought to arise from the collision of the expanding SNR shell with an unassociated nebula near the position of the star γ-Cygni (see Lozinskaya 1992 for a review). The X-ray emission is complex and is possibly correlated with the radio emission in the region of the γ-Cygni nebula (Higgs et al. 1983). From the X-ray data, Higgs et al. (1983) infer a density of $>$0.7 cm^{-3} consistent with the post-shock gas density of 2 cm^{-3} derived by Landecker, Roger & Higgs (1980 [LRH]). From CO emission lines, dense molecular clouds shocked by the expanding SNR shell have been identified (LRH; Cong 1977; Fukui & Tatematsu 1988). The positions of these clouds have been found to be roughly consistent with cooler regions or holes in the X-ray emission (Higgs et al. 1983). Contours of the 110 GHz CO emission line intensity from Fukui and Tatematsu (1988) are shown in Fig. 3b. LRH and Pollock (1985) estimate the gas density in the molecular cloud to be $n \approx 100 - 300$ cm^{-3}. ADV estimate a filling factor of $\Delta V/V \approx 0.05$ giving a volume average value for n of as much as $n \approx 15$ cm^{-3}. Another density estimate obtained from the three-dimensional matter distribution derived by Bertsch et al. (1993) gives n=1.1 cm^{-3} (Esposito et al. 1996). Thus a reasonable range of densities for this remnant is $n \approx 1.1 - 15$ cm^{-3}. Observations by Landecker et al. (1980) show evidence for accelerated H I associated with the remnant and from this association derive a distance of $\approx$1.5 kpc for the remnant. Both the surface brightness and the kinematic distance to an associated H II region (Lozinskaya 1992) suggest a similar distance of $\sim$1.8 kpc. Sturner & Dermer (1994) and Higgs et al. (1977) estimate an age of 5400 and 10000 years respectively, derived from the angular size and distance to the remnant. The SNR is most likely in its adiabatic expansion phase during which period the γ-ray flux should be near its maximum value (DAV). With $\theta \approx 0.15$, $nE_{\rm SN} \approx 1.1 - 15.0 \times 10^{51}$ erg cm^{-3} and a distance $d \approx 1.5$ kpc we estimate $\mathscr{A} \approx 0.07 - 1.0$.

2.4. G189.1+3.0 (IC443)

IC443 is a radio shell SNR with an angular extent of 45′ and a flux of 160 Jy at 1 GHz (Green 1995; see the contours in Fig. 4b taken from Green 1986). The radio spectrum is nonthermal and has an average spectral index of 0.36 in the northeast (Erickson and Mahony 1985) but varies across the remnant from a a relatively hard broken spectrum in the northeast, to a softer power-law spectrum with $\alpha \sim 0.4 - 0.66$ in the fainter southwest (Green 1986; Braun & Storm 1986). The latter spectrum is roughly consistent with the expectations for Fermi-accelerated electrons (e.g., Ellison & Reynolds 1991). Recent ASCA observations reveal nonthermal X-ray emission in two regions on the radio shell (a compact region and a ridge of emission both in the southeastern rim) where the shock is also apparently interacting with a molecular cloud. These data are interpreted as giving evidence for the shock acceleration of cosmic-ray electrons up to energies of $\sim$10 TeV.

Based on the assumed connection with the H II region S249, Fesen (1984) derives a distance of 1.5 to 2 kpc, consistent with the kinematic distance of 0.7-1.5 kpc derived from the radial velocity of the outermost filaments in the remnant (Lozinskya 1992).

The enhanced brightness and small radius of curvature of the shock front in the northeast of the remnant provides strong evidence for an association of IC443 with dense clouds in this region (e.g., Lozinskaya 1992). The gas in this region has an average density of n = 10 $-$ 20 cm^{-3} and contains dense knots with n = 100 $-$ 200 cm^{-3} (Lozinskaya 1992). The SNR is also

thought to interact with a dense molecular cloud ring which extends from the northeast and covers the southern part of the remnant, obscuring the X-ray emission in that region. One contour of the CO emission taken from Cornett et al. (1977) is shown in Fig. 4b. That the SNR shell is interacting with the cloud is based on numerous observations of shocked cloudlets with velocities and velocity dispersions similar to that of the remnant (e.g., Lozinskaya 1992; DeNoyer 1979a; DeNoyer 1979b; DeNoyer & Frerking 1981). In fact the detection of shocked molecular gas in IC443 provides the strongest evidence for any SNR of an interaction with a dense cloud. The mean density of the molecular cloud has been estimated to be as much as $n \gtrsim 200$ cm^{-3} (Cornett et al. 1977; Scoville et al. 1977) to 500 cm^{-3} (Treffers 1979).

The X-ray emission peaks inside the radio shell and fills the northeastern and eastern portions of the remnant (Petre et al. 1988; Rho 1995). From data taken with the ROSAT PSPC and assuming a distance of 1.5 kpc, Rho (1995) derives an age of 6200 yr, an explosion energy of 1.1×10^{51} erg and an average density of 1.1 cm^{-3}. From data taken with the SSS, IPC and HRI instruments on the *Einstein Observatory*, Petre et al. (1988) derives an age of ∼3000 yrs, an explosion energy ranging from $0.5 - 4.0 \times 10^{51}$ ergs and an average density ranging from $\sim 5-20$ cm^{-3}. We take the reasonable range of densities to be $n \approx$ 1.1 to 20.0 cm^{-3}. Using $nE_{\rm SN} \approx 1.2 - 20.0 \times 10^{51}$ erg cm^{-3} $d \approx 1.5$ kpc and $\theta \approx 0.15$, one obtains $\mathscr{A} \approx 0.08 - 1.3$.

The strongest case for an association with an EGRET unidentified source (2EG 0618+2234) has been made for this SNR. The EGRET source has an integral flux above 100 MeV of $5.0 \pm 0.4 \times 10^{-7}$photons cm^{-2}s^{-1} and a differential spectral index of $\alpha = 1.97 \pm 0.07$ (Esposito et al. 1996).

2.5. G34.7-0.4 (W44)

W44 is a radio shell-type SNR with an angular extent $35' \times 27'$ and radio flux of 230 Jy (e.g., see the radio contours from Clark et al. (1975) shown in Fig. 5b). X-ray data from the *Einstein Observatory* and the ROSAT PSPC show a centrally peaked X-ray morphology. A radio pulsar PSR B1853+01 (Wolszczan et al. 1991) is associated with the remnant. Harrus et al. (1996) have concluded that a hard X-ray source detected with ASCA corresponds to an X-ray synchrotron nebula associated with the pulsar. W44 is also thought to be interacting with dense molecular clouds (Wootten 1977; DeNoyer 1983). In Fig. 5b, one contour of the CO column density map of Wootten (1977) is superimposed on the contours of the continuum radio emission. The lack of X-ray emission along the eastern limb within the radio shell has been interpreted as due to obscuration of the remnant by a large molecular cloud (Rho et al. 1994).

A reliable distance of 3 kpc has been determined from H I and OH absorption (Green 1984). From the X-ray data, Rho et al. (1994) derive an age of 6000 yr, which is smaller than the pulsar age of 2×10^4 yrs (Wolszczan et al. 1991). Estimates for the initial density in the pre-shocked intercloud gas range from 0.1 to 0.7 cm^{-3} (Rho et al. 1994), and $\gtrsim$20-200 cm^{-3} for the pre-shocked density of the gas in the cloud component (Lozinskaya 1992; Wootten 1977). A canonical explosion energy of 10^{51} ergs is assumed. Esposito et al. (1996) derive a value of $n \approx 2.4$ cm^{-3} from the model of Bertsch et al. (1993). Using $nE_{\rm SN} \approx 0.7 - 10.0 \times 10^{51}$ erg cm^{-3}, $d \approx 3.0$ kpc and $\theta \approx 0.15$, we estimate that $\mathscr{A} \approx 0.01 - 0.17$.

The EGRET unidentified source 2EG 1857+0118 with $F(>$ 100 MeV) = $64.3 \pm 13.3 \times 10^{-8}$ photons cm^{-2}s^{-1} (Thompson et al. 1995) is consistent with the position of this remnant. Fierro (1996) derives a hard spectrum with $\alpha = -1.90 \pm 0.16$ for the unidentified source. No pulsed emission at the period of PSR 1853+01 has been found (Esposito et al. 1996).

2.6. G49.2-0.7 (W51)

W51 is a radio bright (∼160 Jy) SNR with a shell-like radio structure with an angular extent of $30'$ (Green 1995) as shown in Fig. 6b taken from the 4850 MHz survey of Condon et al. (1994). Polarization measurements (Velusamy & Kundu 1974) as well as measurements of a flat nonthermal spectrum with $\alpha \approx -0.26$ (Moon & Koo 1994) demonstrate that the radio emission is nonthermal, consistent with the interpretation of W51 as a supernova remnant. The X-ray structure is complicated, showing both center-filled and shell-type X-ray morphologies. In the southeast the X-ray structure matches that of the radio shell fairly well, although the peak nonthermal radio emission actually falls within the X-ray shell. A large fraction of the thermal component of the radio emission comes from two compact H II regions within the angular extent of the radio shell. Koo & Moon (1997) have identified shocked H I gas at an interface between the X-ray bright central region of the W51 SNR and a large molecular cloud. Contours of the CO emission from Koo & Moon (1997) are shown in Fig. 6b (the shocked H I gas lies in the center of this region). The preshock density of the molecular cloud is estimated to be ∼200 cm^{-3} from the CO data, and the measured shock velocity is consistent with the expectations for a large molecular cloud overtaken by the strong supernova blast shock. Since W51 is located at a tangential point of the Sagittarius arm it is a very complex region of the sky, and the unusual X-ray and radio structure of the remnant may be due to the chance overlap of several objects (Koo, Kim & Seward 1995 [KKS]). However, Koo & Moon (1997) also suggest that the complex structure of W51 could be explained as resulting from the explosion of the supernova taking place within or near a large molecular cloud.

There are no reliable distance estimates for this remnant (Green 1984). Sato (1974) derive a value of $d = 4.1$ kpc from the Maryland Greenbank H I survey. The $\Sigma - D$ relation (where the radio surface brightness Σ and angular size of the remnant D are used to derive a distance) gives a distance of 2.5 kpc according to Montmerle (1979), but such estimates are unreliable (e.g., Green 1984). KKS put the remnant behind the high-velocity molecular stream seen in this region which has an estimated distance of 5.6 kpc based on an association with a high velocity H I region (Burton & Shane 1970).

Assuming that W51 is a single SNR at a distance of 6 kpc and using a Sedov model, KKS derive a high explosion energy

Table 1. Properties of Candidate Gamma-Ray Sources

									EGRET ($E > 100$ MeV)		
	Gal. Coords			Flux[a] 1 GHz	Age	Dist.	n×E_{51} (cm^{-3}×		Source	Integral Flux (10^{-7}	Spectral Index
Name	l	b	Size[a]	(Jy)	(yr)	(kpc)	10^{51}erg)	Type[a†]	ID	cm^{-2}s^{-1})	α
W44	34.7	−0.4	35′ ×27′	230	6000–20 000[c]	3.0±1.0[k]	0.7[c]–10	C[c]	J1857 +0118	6.4±1.3	1.9±0.16[p]
W51	49.2	−0.7	30′	160?	30 000[n]	2.5[d]–6.0[n]	0.47[n]–36	C[n]		2.9σ[b*]	
γ-Cygni	78.2	+2.1	60′	340	5400[e]–10 000[g]	1.5[f]–1.8[j]	1.1[b]–15[h]	S	J2020 +4026	12.6±0.7	2.07±0.05[b]
W63	82.2	+5.3	95′ ×65′	120?	24 000[i]	1.5–2.0[i]	0.07[i]–1.0	S		2.6σ[b*]	
Tycho	120.1	+1.4	8′	56	425	2.3±0.5[k]	0.20[l]–3.2[m]	S			
IC443	189.1	+3.0	45′	160	3000[n]–6200[i]	1.5–2.0[o]	1.2[i]–20[q]	S	J0618 +2234	5.0±0.4	1.97±0.07

[a]Green 1995, [b]Esposito et al. 1996, [c]Rho et al. 1994, [d]Montmerle 1979, [e]Sturner and Dermer 1995, [f]Landecker, Roger & Higgs 1980, [g]Higgs 1977, [h]Aharonian 1994, [i]Rho 1995, [j]Lozinskaya 1992, [k]Green 1984, [l]Hamilton et al. 1986, [m]Heavens 1984, [n]Koo, Kim & Seward 1995, [o]Fesen 1984, [p]Fierro 1996, [q]Petre et al. 1988

[†]Type definitions: S=shell, C=composite (shell-like radio morphology with centrally concentrated X-rays)

[*]Not in second EGRET catalog, significance of emission is given.

of 3.6×10^{51} ergs. From the temperature of the X-ray emitting gas and the shock jump conditions, KKS derive a shock velocity of $v_S \approx 490$ km s^{-1} which combined with the angular size and assumed distance yield an age of 3.0×10^4 yrs. Using the Sedov model, KKS derive an ambient intercloud density of $n_{\rm H} = 0.13$ cm^{-3}. The centrally peaked X-ray emission could arise from evaporation of embedded dense clouds, from synchrotron radiation from a central plerion (the ROSAT spectrum cannot distinguish between thermal and nonthermal emission) or the chance coincidence of another SNR. For this remnant we estimate $\mathscr{A} \approx 0.002 - 0.15$, taking $E_{\rm SN} \approx 3.6 \times 10^{51}$ ergs, $d \approx 6.0$ kpc, $n \approx 0.13 - 10.0$ cm^{-3} and $\theta \approx 0.15$.

A small excess of 2.9σ is seen in the EGRET data (Esposito et al. 1996). While normally this would not be considered significant, this and the other SNRs described in this section were selected for observation before the EGRET results were obtained there by providing an a priori hypothesis for emission.

2.7. G82.2+5.3 (W63)

W63 is a radio shell remnant with an angular size of $95'\times65'$ and surface brightness of ∼120 Jy (Green 1995). Radio contours derived from the 4850 MHz survey of Condon et al. (1994) are shown in Fig. 7b. The observations of Velusamy & Kundu (1974) indicate polarization consistent with a nonthermal origin of the radio emission. The remnant has a radio spectral index of $\alpha \approx 0.5 - 0.77$ (Higgs et al. 1991; Angerhofer et al. 1977). The distance is estimated to be approximately 1.6 kpc using the $\Sigma - D$ relation (Rosado & Gonzalez 1981) but is estimated to be greater than 2 kpc from optical reddening of associated optical filaments (Wendker 1971). The remnant has a filled X-ray structure which is anticorrelated with the radio emission (Rho 1995). From the Sedov and evaporation model Rho (1995) derives an age of 2.4×10^4 yrs, a pre-shocked intercloud density of $n_0 = 0.06 - 0.17$ cm^{-3} and a blast energy of 0.6×10^{51} erg at an assumed distance of 2 kpc. Rosado & Gonzalez (1981) derive values for E/n_0 from measurements of the radial velocity field of optical filaments ranging from 10^{49} to 5×10^{51} erg cm^3 implying densities ranging from $n_0 = 0.2 - 100$ cm^{-3}. Lacking good information on the density, we adopt a more typical value for the upper value of the ISM density of 1.0 cm^{-3} giving $nE_{\rm SN} \approx 0.07 - 1.0 \times 10^{51}$ erg cm^{-3} at $d \approx 2.0$ kpc. Taking $\theta \approx 0.15$ we estimate that $\mathscr{A} \approx 0.003 - 0.04$. As is the case for W51, a small positive excess of 2.6σ is seen in the EGRET data (Esposito et al. 1996).

2.8. G120.1+1.4 (Tycho)

Tycho is distinct from the other objects on our list in that it is younger than the other SNRs and has both a shell-like radio and X-ray morphology. Since Tycho has a small angular size $\approx 8'$ it is ideally suited to traditional observations with atmospheric Čerenkov telescopes. Tycho has a 1 GHz flux of 56 Jy and spectral index of -0.61. The spectral index and spectral shape are found to be in good agreement with the predictions of the nonlinear shock acceleration model of Reynolds & Ellison (1992). Tycho is an historical SNR (AD 1572) and the optical light curve is sufficiently well defined that it can be classified as a type Ia supernova. Distances estimated by comparing the absolute magnitude for type Ia supernovae to the apparent magnitude (Chevalier et al. 1980) and by proper motion studies (Kamper & van den Bergh 1978; Strom et al. 1982) give a reliable value of $d = 2.3 \pm 0.5$ kpc (Green 1984). Proper motion studies also show that despite its young age, the remnant has been significantly decelerated and hence is near the Sedov phase of expansion (see also Tan & Gull 1985). From calcula-

tions of the swept-up mass derived from high resolution X-ray observations made with the *Einstein Observatory*, Seward et al. (1983) have also concluded that the SNR is at an evolutionary stage between uniform and adiabatic expansion.

X-ray models give estimates for the density and explosion energy varying from n = 0.28 cm^{-3} and $E_{\rm SN}$ = 7 × 10^{50} erg (Hamilton et al. 1986) to n = 1.13 cm^{-3} and $E_{\rm SN}$ = 1.9 × 10^{50}erg (Smith et al. 1988). Heavens (1984) calculates a dynamical value for $E_{\rm SN}/n \approx 0.2 \times 10^{51}$ erg cm^3 from radio and X-ray data, similar to that derived by Smith et al. (1988), but derives an explosion energy of $E_{\rm SN} = 8 \times 10^{50}$ erg (closer to the canonical value) which gives an ambient density of 4 cm^{-3}. Huang & Thaddeus (1986) report a spatial coincidence with a molecular cloud but question the evidence presented by Cornett (1977) for shocked CO which would indicate an interaction between the SNR and the molecular cloud. Using $nE_{\rm SN} \approx 0.2 - 3.2 \times 10^{51}$ erg cm^{-3}, $d \approx 2.3$ kpc and $\theta \approx 0.15$ one obtains $\mathscr{A} \approx 0.006 - 0.09$. No significant excess is seen in the EGRET data from the direction of this SNR.

3. Data analysis

The standard Whipple data analysis procedures are discussed in detail elsewhere (e.g., Reynolds et al. 1993). Here we discuss those aspects of the data analysis which have been modified to analyze the data from extended galactic-plane sources. A more detailed discussion of these methods will be given in a companion paper Lessard, Buckley & Connaughton (1997).

3.1. Compensation for sky brightness

Data are taken in a differential mode where each 28 min ON-source run is followed by a 28 min OFF-source control run which is offset in right ascension to ensure that the same range of azimuth and zenith angles are sampled. While this cancels the zenith angle dependence of the cosmic-ray rate as well as other systematic effects in the camera, differences in sky brightness between the ON-source and OFF-source regions can lead to biases. For some galactic plane sources, such differences are substantial due to either diffuse emission from the galactic plane or bright stars.

Systematic effects arising from such brightness differences can be largely canceled by the following procedures: during data taking, high voltages of photomultiplier tubes (PMTs) affected by the presence of a bright star are turned off both in the ON-source and OFF-source observations. To determine the brightness level in each pixel, the rms deviations in the PMT pulse height distributions for artificially injected triggers are determined. In the data analysis software, noise is added to all pixels of each event so that matching PMTs in ON-source and OFF-source runs have identical noise pulse height spectra (Cawley et al. 1990). Only PMT signals which exceed some multiple of this noise level are included in the subsequent analysis of the shower images (Punch et al. 1991).

Since sub-threshold events can be promoted above the hardware trigger threshold by the addition of random noise, the software trigger threshold is set above the hardware threshold by several standard deviations of the noise pulse height distribution. Because the SNR data were obtained over different epochs with variations in PMT gains and light collection efficiency, the software trigger threshold was also adjusted to give roughly equivalent energy thresholds of 300 GeV for each observing season. The resulting threshold corresponds to the approximate trigger condition that the signals in two PMTs exceed 70 photoelectrons.

Based on numerous control data sets, the residual systematic error after application of this procedure is found to be significantly lower than the level of statistical fluctuations. However, the additional noise in the data increases the energy threshold, and zeroing phototubes decreases the effective area. To quantify these effects, noise was added to a Crab data set to exactly match the level present in the γ-Cygni exposures (which had the brightest background light levels), and identical PMTs were zeroed in the analysis. The significance of the detection and the γ-ray rate derived from the Crab data were marginally degraded. From this test we make a quantitative estimate of a $\lesssim$10% systematic error separately on both the effective energy threshold and the effective area.

The effective energy threshold and effective area are determined from Monte Carlo simulation (see Mohanty et al. 1997; Connaughton 1996). From comparisons of different simulations and different calibration procedures, we estimate the systematic uncertainty in the energy threshold to be $<$20%.

3.2. Extended source analysis

In order to analyze the data from extended sources, a new data analysis technique was developed to derive an approximate point of origin on the sky for each γ-ray shower. This method is described in detail in a companion paper Lessard, Buckley & Connaughton (1997) and is based on the methods described by Reynolds et al. (1993) and Akerlof et al. (1991). After initial processing of the shower images including pedestal subtraction, gain correction and image cleaning (e.g., Punch et al. 1991), individual Čerenkov shower images are subjected to a moment analysis to determine a set of simple parameters that characterize the images (e.g., Reynolds et al. 1993). Two of the parameters, *length* and *width*, specify the roughly elliptical shape of the images by the RMS spread of light along the major and minor axes, respectively. γ-ray showers give rise to more compact images than background hadronic showers and can be efficiently selected based on these shape parameters with a background rejection factor of $\sim$20.

Once these candidate γ-ray events have been selected, additional characteristics of the shower images can be used to determine the most likely point of origin of a γ-ray shower. Monte Carlo simulations show that the *elongation* of the shower image (i.e., *length/width*) and the angular distance between the centroid of the shower image and the source position *dist* both increase with increasing impact parameter of the air shower (e.g., Akerlof et al. 1991). The parameter α is defined as the angle between the major axis of the shower image and a line from its centroid

to the assumed source location in the image plane. The most likely source position is found to lie along the major axis of the shower ($\alpha = 0$) at an angular distance from the image centroid of $dist = 1.7 \times (1 - width/length)$. The remaining ambiguity in the source position can be resolved from an additional parameter *asymmetry* derived from the third moment of the light distribution (Lang 1991; Punch 1993). Shower images generally have a cometary shape with their light distribution skewed towards their point of origin in the image plane (positive *asymmetry*). Lang (1991) and Punch (1993) have shown from data taken on the Crab Nebula that γ-ray images point fairly unambiguously towards their point of origin. From these parameters, a unique point of origin of each shower can be determined, and the emission over an extended region can be calculated by summing the number of excess events in this region. To illustrate this technique, Fig. 1 shows two candidate γ-ray events taken from a data run on the Crab Nebula along with possible points of origin derived from the image parameters.

Analysis of data taken on the Crab Nebula indicates that the point spread function for localizing the origin of the γ-ray showers can be approximated by a two-dimensional Gaussian function:

$$\frac{dN}{d\Omega} = \frac{1}{2\pi\sigma^2} \exp\left(\frac{-\theta^2}{2\sigma^2}\right) \tag{2}$$

where σ =0.°13. Assuming a uniform background, it is then straightforward to derive that the optimum significance for a point source is obtained by binning points within a circular region of radius 1.59σ which keeps 72% of the γ-ray counts.

To produce plots of the γ-ray emission and to provide a test for the presence of significant emission anywhere within the field of view, the points are rebinned according to a different procedure. First the parameters *length*, *width* and *elongation* are determined for each event. Parameters which depend on the assumed source position (i.e., the angle α, *dist* and *asymmetry*) are recalculated with respect to each point on a 30×30 grid. If the data selection criteria given in Table 2 are satisfied at a given grid point, then the number of candidate events at that grid point (N_i) is incremented (e.g., see Fig. 1). For each grid point, the number of candidate events ON-source ($N_{\rm on}$) and OFF-source ($N_{\rm off}$) can then be used to derive the excess number of events (number of γ-rays). The likelihood ratio λ compares the null hypothesis that the observed number of counts arise from background to the hypothesis that an additional source component is present (Li & Ma 1983):

$$\lambda = \left[\frac{1}{2}\left(\frac{N_{\rm on} + N_{\rm off}}{N_{\rm on}}\right)\right]^{N_{\rm on}} \left[\frac{1}{2}\left(\frac{N_{\rm on} + N_{\rm off}}{N_{\rm off}}\right)\right]^{N_{\rm off}}. \tag{3}$$

If the source position is hypothesized at one particular grid point then $-2\ln\lambda$ is distributed asymptotically as χ^2 with one degree of freedom, and the statistic $S_\lambda = \sqrt{-2\ln\lambda}$ is equivalent to the significance in units of σ. The values of $N_{\rm on}$, $N_{\rm off}$ and S_λ can be used to provide an image of the γ-ray emission from an extended source, and to indicate the presence of any compact features or point sources within the field of view.

To test this method and test the Monte Carlo predictions for the γ-ray efficiency, three Crab data sets were analyzed (see Fig. 2). Fig. 2a shows the first data set derived from 84 minutes of data obtained with the telescope pointing at the Crab. Fig. 2b shows a similar 84 minute data set but with the telescope pointing 0.°4 offset in declination from the Crab Nebula position. Archival data with a 1° offset are also shown (Fig. 2b). These data were taken at a substantially higher energy threshold (560 GeV) but with a longer exposure (570 min). In these two-dimensional plots, the gray-scale indicates the number of excess counts (candidate γ-rays) after smoothing and the contours shown correspond to the statistic S_λ in steps of 1.

Monte Carlo simulations demonstrate that the source position can be reconstructed using this technique across the entire 3° field of view, but with a declining γ-ray efficiency as the source position is moved out from the center of the field of view (Connaughton 1996). From simulations, the effective area falls off gradually from a peak value of 2.3×10^8 cm^2 for a point source at the center of the field of view to 2.0×10^8 cm^2 for a source 0.°4 away (Lessard 1997). The relative variations in the γ-ray efficiencies measured from the offset Crab data are completely consistent with the results of the simulations.

To make a quantitative measure of the upper limit on emission from an extended region, the most likely points of origin are directly binned on a two dimensional grid. Depending on the angular size of the source, an appropriate aperture (defined below) is applied to the two-dimensional grid to determine the excess number of candidate γ-ray events within the extended region. For the present analysis, this aperture has a radius equal to the radius of the radio shell, $r_{\rm S}$, plus two times the width of the two dimensional point spread function, that is $r_{\rm S} + 2\sigma$. To be conservative, this radius was chosen to be slightly larger than the optimum value $r_{\rm S} + 1.59\sigma$.

The total number of counts ON-source and OFF-source within this aperture are combined to give $N_{\rm on}$ and $N_{\rm off}$. An upper limit to the number of counts $N_{\rm u.l.}$ is derived according to the method of Helene (1983). The upper limit corresponds to the maximum value for μ (the mean number of counts of the parent Poisson probability distribution) for which the observed values of $N_{\rm on}$ and $N_{\rm off}$ are still consistent at the 99.9% confidence level.

For some sources we have combined the results of exposures taken at different pointing directions. The calculation of the effective collection area of the telescope for an extended source takes into account the reduced detection efficiency away from the camera center as determined by Monte Carlo. For simplicity, we assume that the γ-ray emission is uniform over the extent of the SNR. For each pointing direction, the effective area function is numerically integrated over the region covered by the SNR to derive an average effective area $A_{\rm eff,i}$ and the length of the exposure $T_{\rm i}$ taken at this pointing direction is calculated.

The upper limit is then derived by dividing $N_{\rm u.l.}$ by the total exposure:

$$F(>E) < \frac{N_{\rm u.l.}}{\sum A_{\rm eff,i} T_{\rm i}}, \tag{4}$$

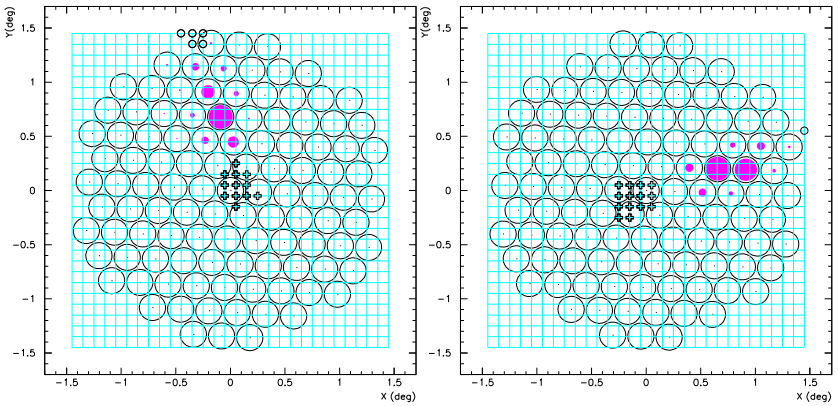

Fig. 1. Two candidate γ-ray events taken from a Crab data run. Pulse heights are shown as varying diameter shaded circles superimposed on the positions of the corresponding photomultipliers. Crosses indicate the positions of possible points of origin distributed about the most likely point of origin, on a two dimensional grid. Open circles represent possible points of origin but with $asymmetry < 0$.

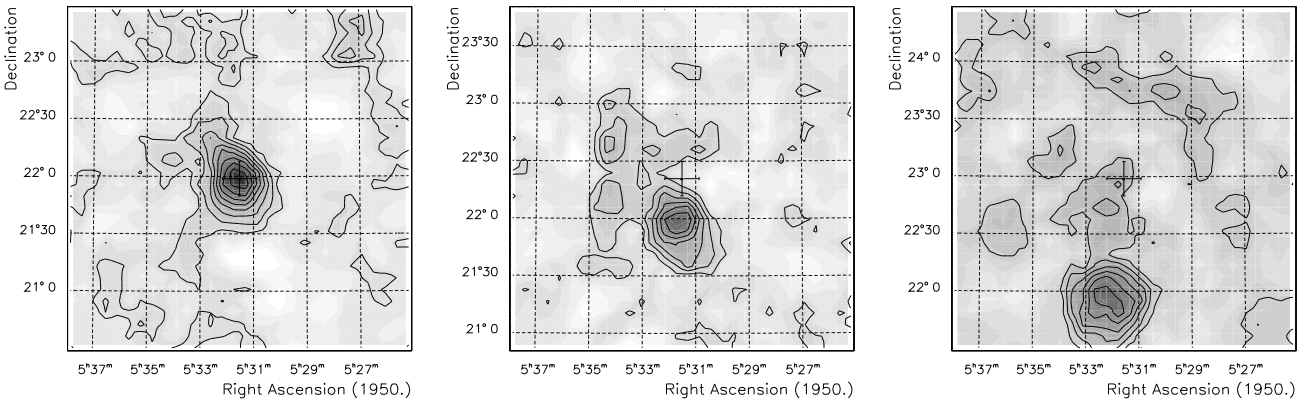

Fig. 2a–c. Results of the analysis described showing smoothed excess γ-ray events (gray scale) and contours of the statistic S_λ for **a** data taken with the telescope pointing at the Crab Nebula, **b** data taken with the telescope pointing offset by $0.^\circ4$ with respect to the position of the Crab and **c** archival data taken with approximately a 1° offset in declination.

Table 2. Cuts used in mesh analysis

Parameter	Lower Bound	Upper Bound
width:	$0.^\circ07$	$0.^\circ15$
length:	$0.^\circ16$	$0.^\circ30$
alpha:	$0.^\circ0$	$10.^\circ0$
dist-1.7×(1-*width/length*):	$-0.^\circ225$	$0.^\circ225$
asymmetry:	0.0	∞

where the sum is over the number of pointings, each with collection area $A_{\mathrm{eff,i}}$ and live time T_{i}.

4. Results

The observations were made over three observing seasons, from 1993 to 1996. During this period there were several incremental changes to the detector arrangement as described by Catanese et al. (1995). Because the SNR data were obtained over different epochs, slightly different software triggers have been used to give approximately the same energy threshold E_{thr} = 300 GeV. Variations in the instrument over these seasons and errors in the calibration of the PMT gain and light collection efficiency are estimated to result in less than a 20% systematic error in the energy threshold.

Two-dimensional images of the γ-ray emission for the extended remnants are shown in Figs. 3-7. For each SNR two figures are shown. The first shows the smoothed distribution of excess (candidate γ-ray) events by the gray scale, together with contours of the statistic S_λ in increments of 1. Also shown on these plots are the elliptical fits to the EGRET 95% error intervals taken from the second EGRET catalog (Thompson et al. 1995). The second plot shows the radio contours superimposed on the distribution of excess candidate γ-ray events, again indicated by the gray-scale. Also shown are the positions of bright stars (with a magnitude scale indicated on the right) to indicate positions where any small residual fluctuations from a systematic effect might be expected. The thick gray contours are taken from CO emission measurements to indicate the position of some of the molecular clouds which probably coincide with the SNRs.

None of the remnants show large excesses at the position of the molecular clouds, at the shell or from point sources within the EGRET error box (see also Buckley et al. 1997). While the apparent excess near the southwest portion of the IC443 shell

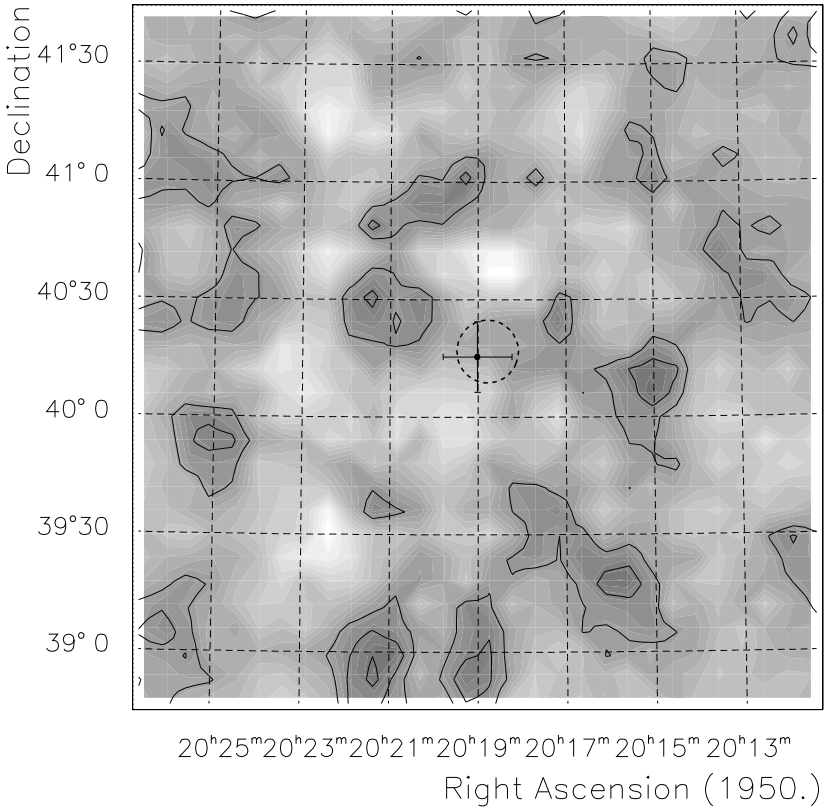

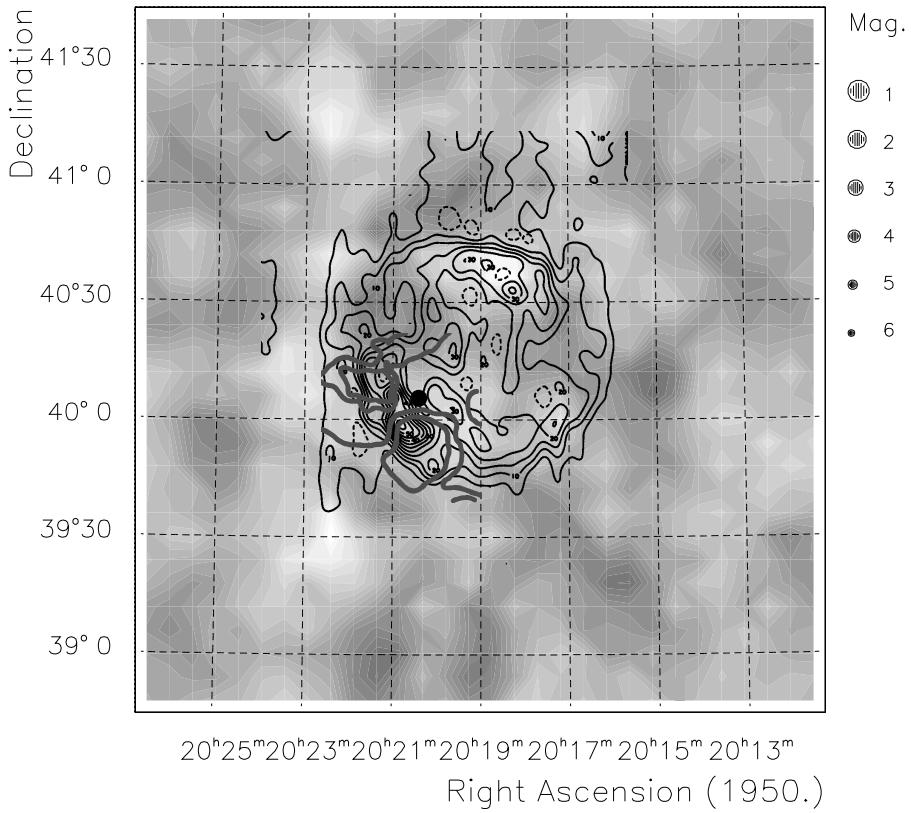

Fig. 3a and b. γ-Cygni: **a** the gray-scale shows the smoothed two-dimensional distribution of excess (candidate γ-ray) events with contours of S_λ, and the EGRET 95% confidence interval indicated by the dashed ellipse; **b** same gray-scale but with radio contours from Higgs et al. (1977) and positions and magnitudes of bright stars indicated. The magnitude of the star is indicated by the diameter of the filled circle as shown in the key to the right of the figure. The thick gray contour is from the CO map of Fukui & Tatematsu (1988) (see main text for other references).

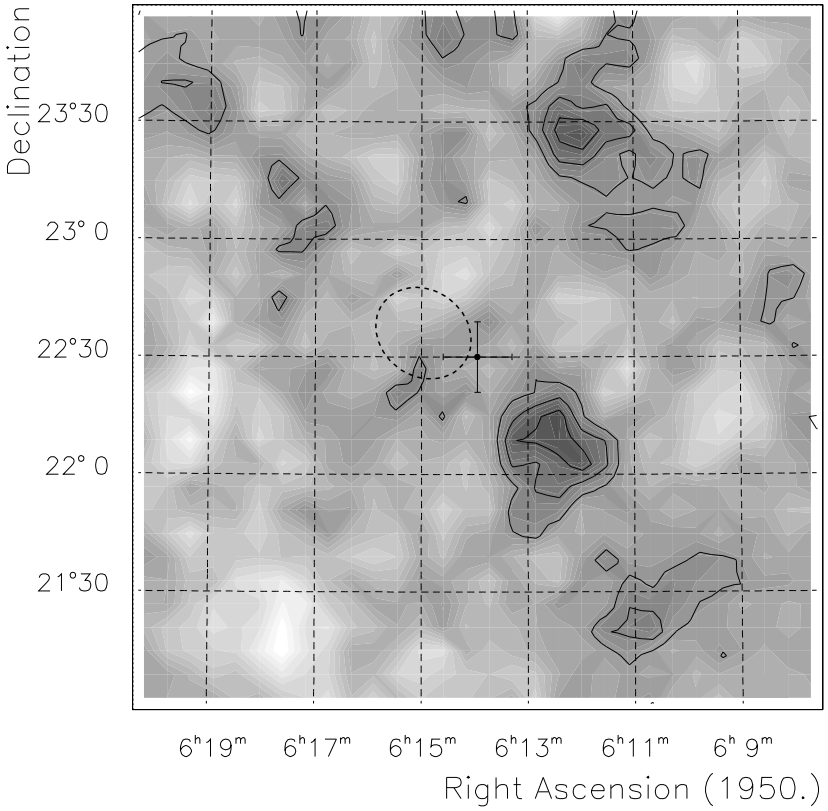

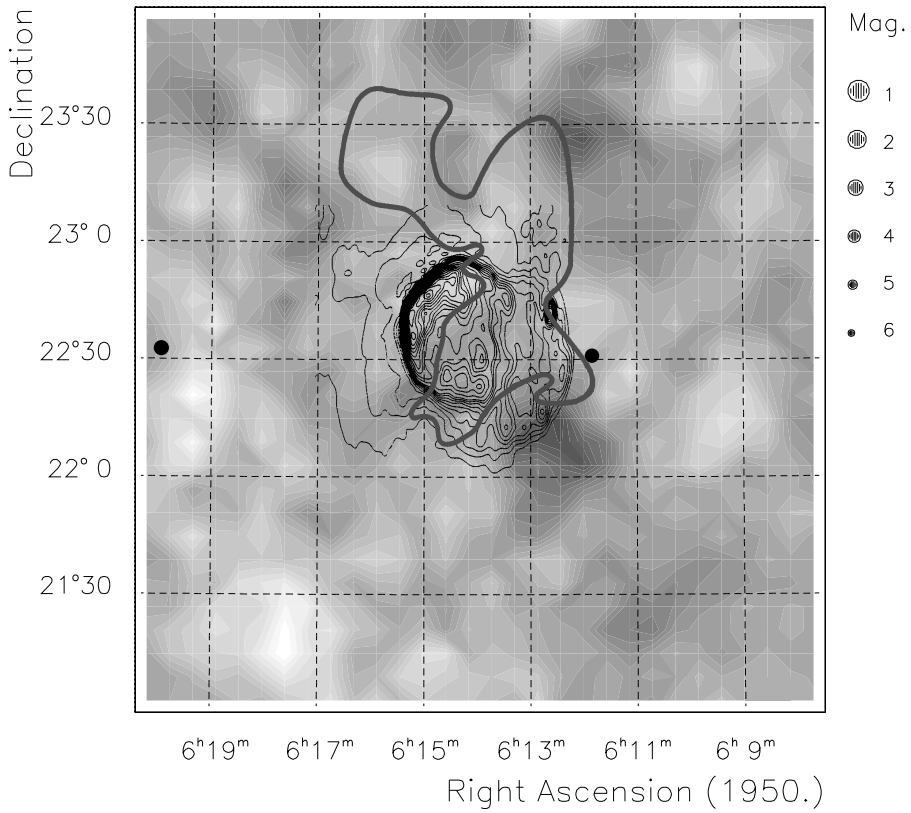

Fig. 4a and b. IC443: **a** two-dimensional distribution of excess (candidate γ-ray) events with the EGRET 95% confidence interval; **b** same with radio contours (Green 1986) and bright stars indicated. The thick gray contour is taken from the CO map of Cornett et al. (1977).

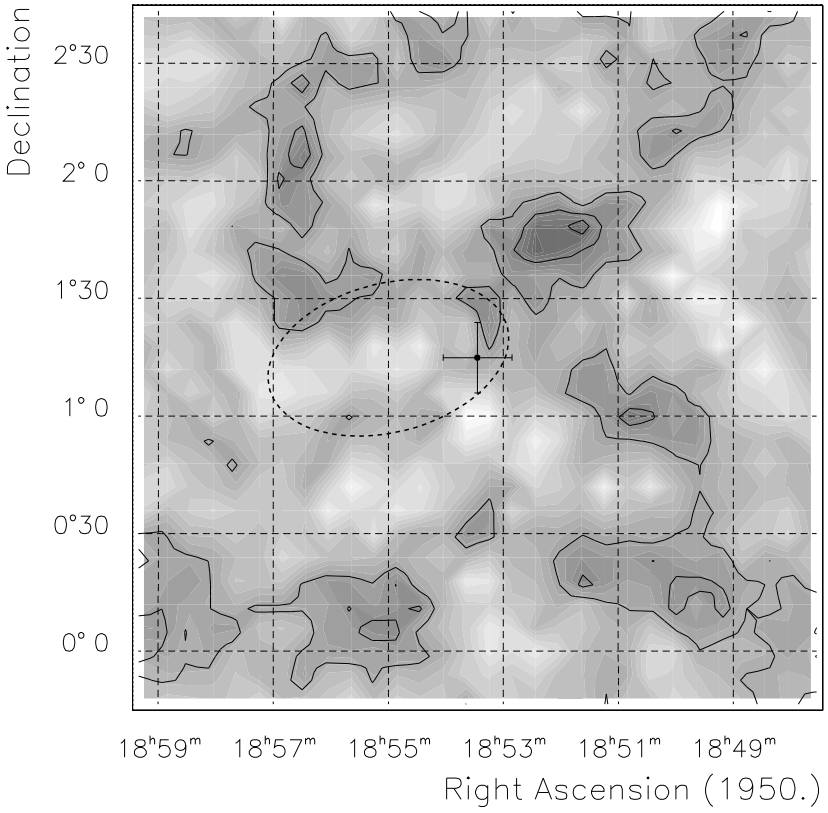

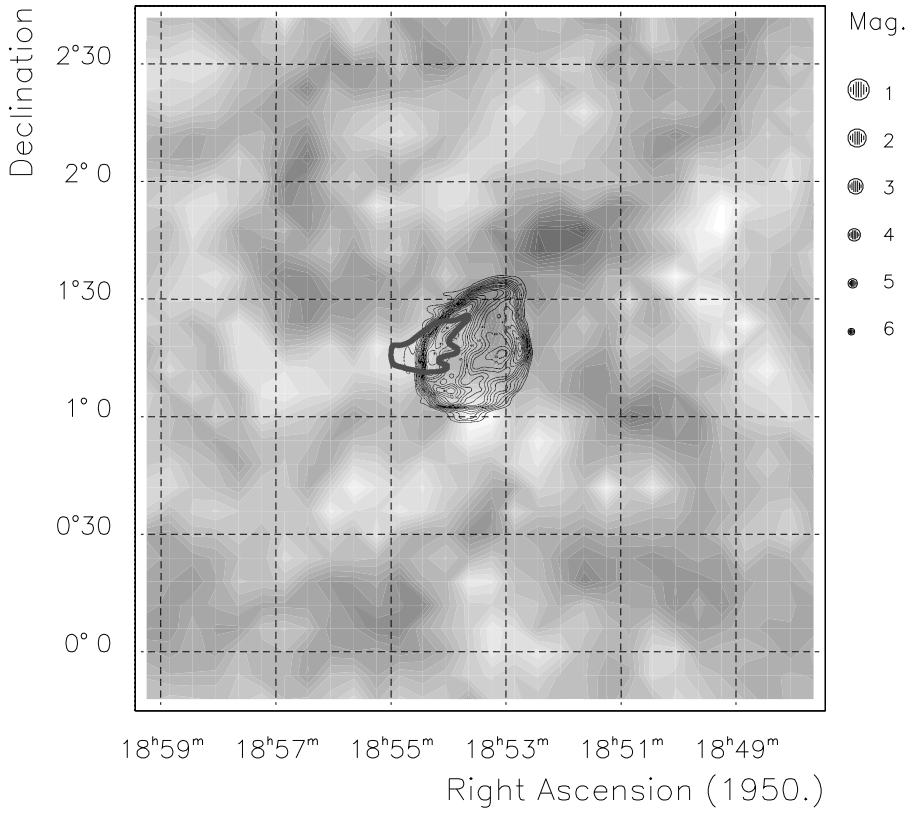

Fig. 5a and b. W44: **a** two-dimensional distribution of excess (candidate γ-ray) events with the EGRET 95% confidence interval; **b** same with radio contours (Clark et al. 1975) and one contour (thick gray line) from the CO map of Wootten (1977) overlayed.

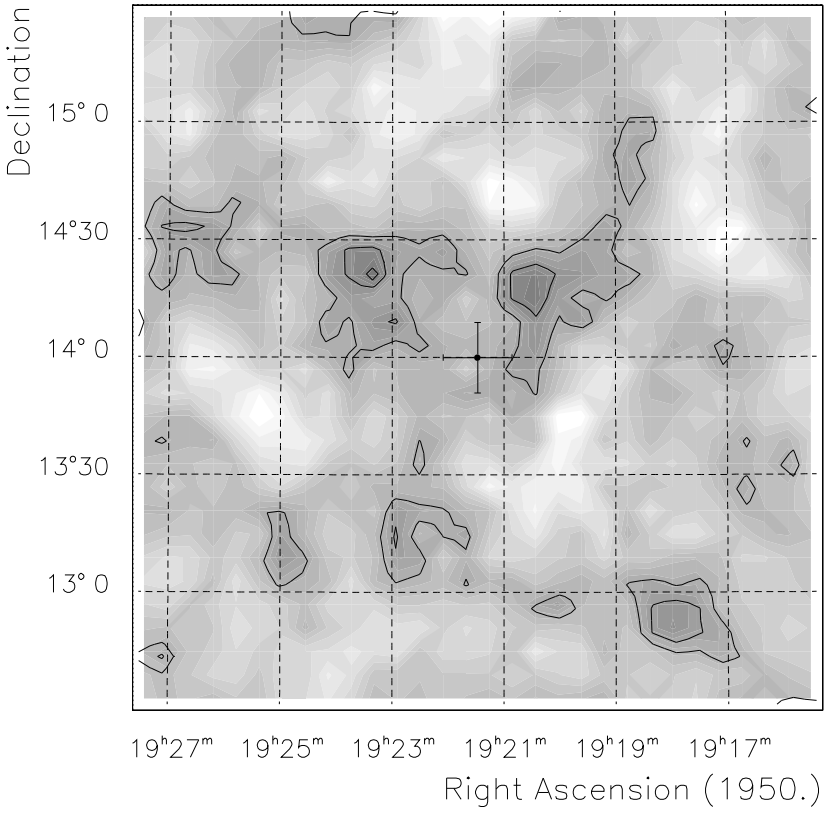

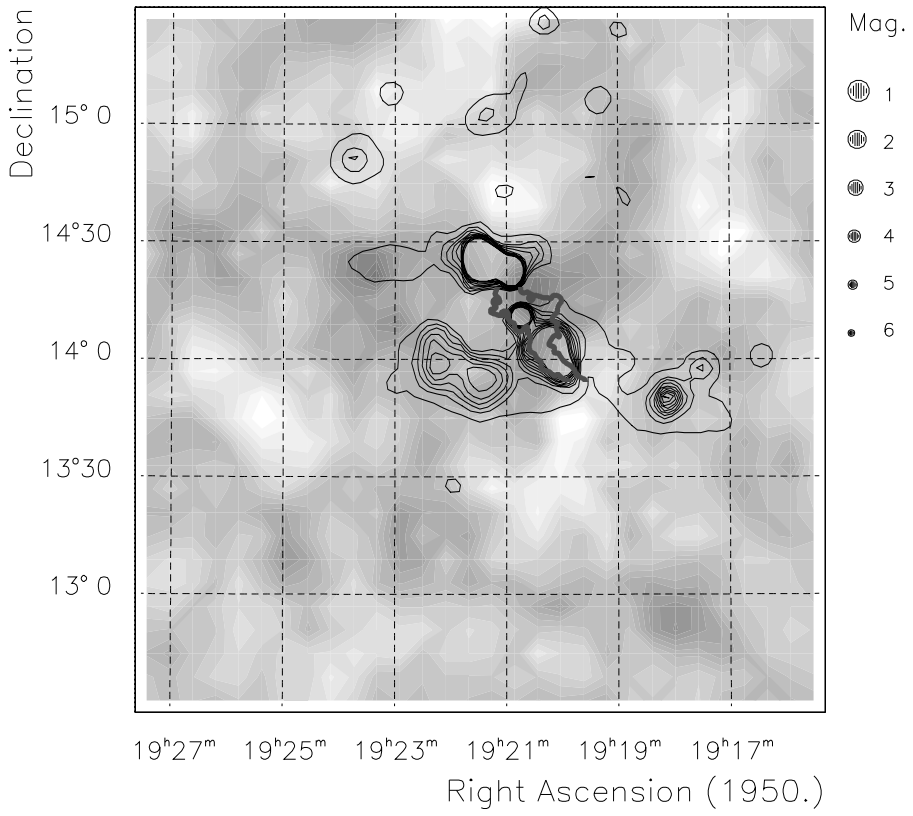

Fig. 6a and b. W51: **a** two-dimensional distribution of excess (candidate γ-ray) events; **b** same with radio contours from Condon et al. (1994) and with one contour (thick gray line) from the CO map of Koo & Moon (1997).

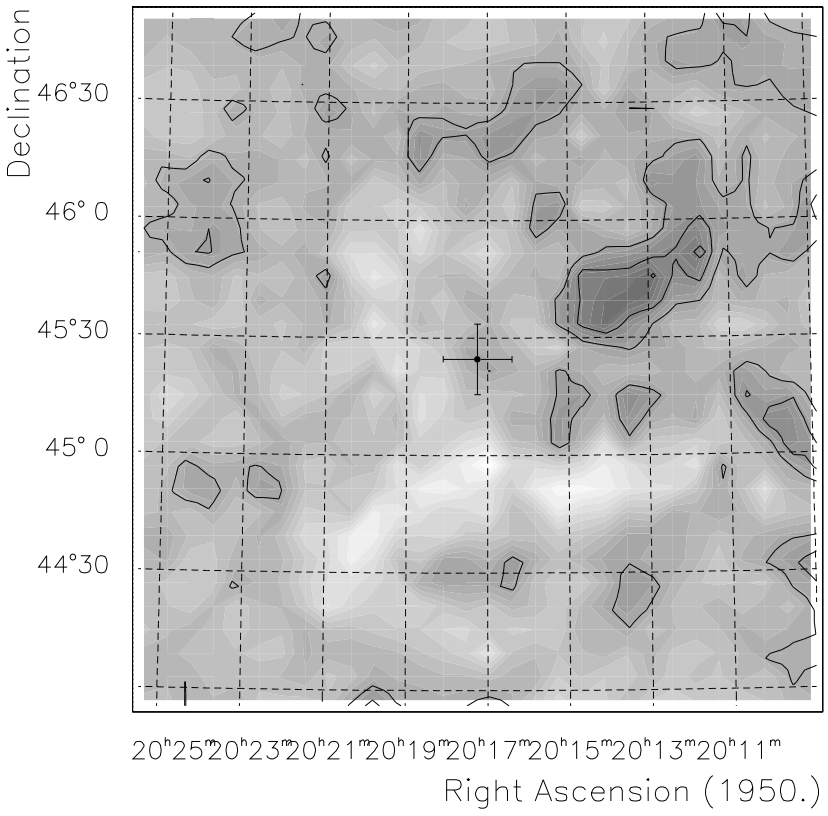

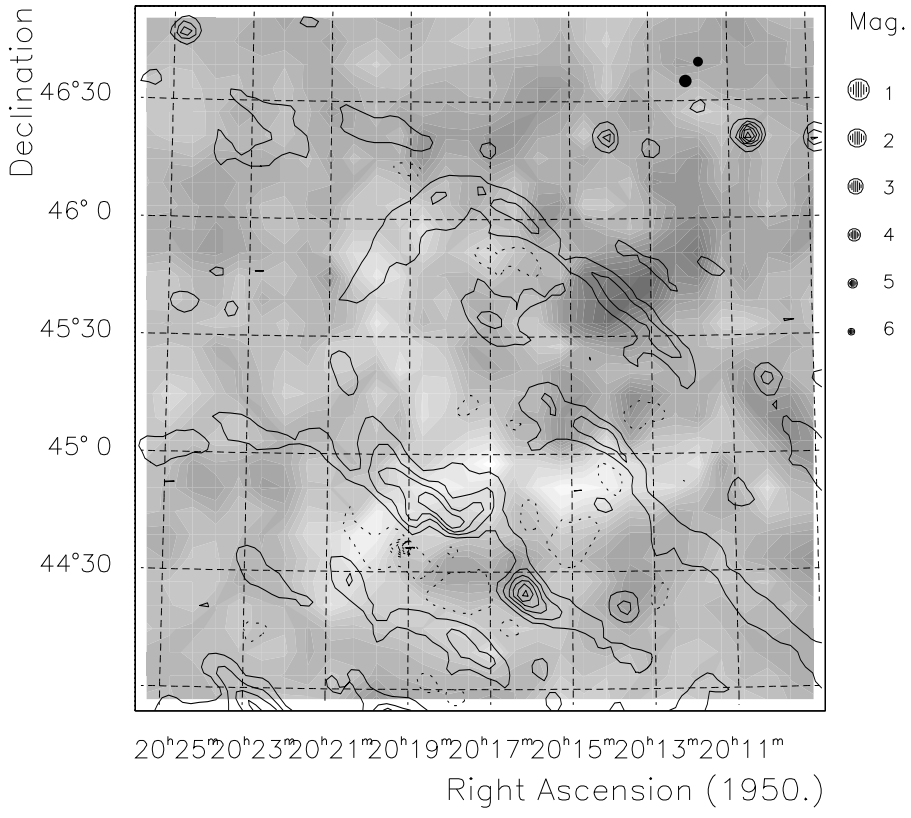

Fig. 7a and b. W63: **a** two-dimensional distribution of excess (candidate γ-ray) events; **b** same with radio contours (Condon et al. 1994) and bright stars indicated.

(Fig. 4) might appear to be significant, it is consistent with expected fluctuations given the large number of trials associated with forming the two dimensional maps. Approximately one $S_\lambda = 3$ excess should occur for each such map on average, and cannot be interpreted as significant in the absence of a prior hypothesis for emission from a particular region. The only evidence for a positive excess at the position of a molecular cloud is in the W51 data. The 2.9σ excess is roughly coincident with the position of the cloud and at the position of the shocked H I gas detected by Koo & Moon (1997), but more data are required to determine the reality of this apparent feature.

In Table 3 quantitative upper limits derived according to the method described in §3.2 are presented along with the circular apertures used for the analysis. In each case the apertures were centered on the position indicated by the cross on the two dimensional plots, at the center of the radio shells. Also indicated in the table are the average effective areas and exposure times for each pointing direction along with the raw number of counts used to derive the upper limits.

5. Model comparison

For simplicity, we only calculate the contribution to the γ-ray flux from protons through π^0-production and neglect possible contributions from primary electrons through electron bremsstrahlung and inverse Compton scattering. The density and spectrum of primary electrons N_e can be derived from the observed radio synchrotron emission if a value for the magnetic field strength is assumed. The bremsstrahlung luminosity $L_{\rm brems} \propto N_e n_0$ where n_0 is the hydrogen density in the ISM. If the energy density of low energy (Comptonized) photons $u_{\rm ph}$ is known, then the IC luminosity can be calculated ($L_{\rm IC}/L_{\rm sync} \propto u_{\rm ph}/u_{\rm B}$ where $u_{\rm B}$ is the magnetic energy density). In order for the shock acceleration model to account for cosmic rays with energies up to $\sim$100 TeV, magnetic field strengths of at least a few μG are required (see equation 6). For magnetic fields of this strength or larger, Sturner & Dermer (1994) calculate for IC443 that the level of the inverse Compton emission should be small compared to the observed EGRET flux, and that without very large ambient densities ($n \gg 10$ cm^{-3}) the electron bremsstrahlung component should also be small. Aharonian, Drury & Völk (1994) also argue that for γ-Cygni that the contribution of protons through pionization probably dominates over the bremsstrahlung component at γ-ray energies above 300 MeV. Because it is possible that electron bremsstrahlung dominates the γ-ray emission given the high densities around these SNR (Gaisser, Protheroe & Stanev 1996), the π^0 component represents a lower limit on the γ-ray emission.

Following Dermer (1986) the γ-ray spectrum dN/dE_γ resulting from the decay of secondary π^0s produced in proton-proton collisions is calculated by numerically integrating the expression

$$\frac{dN}{dE_\gamma} = 8\pi n_0 \int_{E_\gamma+(m_\pi^2/4E_\gamma)}^{\infty} dE_\pi \cdot (E_\pi^2 - m_\pi^2)^{1/2} \times \int_{T_{\rm p}^{\rm min}(T_\pi)}^{\infty} dT_p \cdot j_p(p_p) \cdot \frac{d\sigma(T_\pi, T_p)}{dT_\pi}$$

where $d\sigma(T_p, T_\pi)/dT_\pi$ is the differential cross section for the production of a π^0 of kinetic energy T_π from a proton of kinetic energy T_p colliding with a target proton at rest, n_0 is the number density of target protons, E_π is the total pion energy and m_π is the pion mass. $T_{\rm p}^{\rm min}(T_\pi)$ is the kinematic minimum proton kinetic energy which can result in the production of a π^0 with kinetic energy T_π. The outer integral gives the spectrum of γ-rays resulting from π_0 decay, while the inner integral gives the pion production spectrum. As in Dermer (1986), $d\sigma(T_p, T_\pi)/dT_\pi$ is given by the isobar model of Stecker (1970) with a linear connection to the scaling model of Stephens & Badhwar (1980) at higher energies. The cosmic-ray proton flux is assumed to be a power law in the proton momentum p_p, $j_p(p_p) = j_0 p_p^{-\alpha}$ rather than energy, as indicated by the momentum dependence of the scattering mean free path in shock acceleration models.

Diffusive shock acceleration models generally have difficulty accounting for acceleration to energies much higher than $\sim 3Z10^{14}$eV, however some special circumstances might result in higher energies for some objects (e.g., Völk & Biermann 1988). The break or "knee" in the all-particle spectrum occurs at about the same energy. So while higher energies are possible, for our purpose we make the assumption of a sharp cutoff at momentum $p_{\rm p,max}$ = 100 TeV.

The resulting integral γ-ray spectra are derived by performing the numerical integrations in equation 5 and then normalizing to the predictions of DAV for the integral flux at energies above 1 TeV. The shape of the π^0-decay γ-ray spectrum follows the source cosmic-ray spectrum at high energies > 10 GeV giving a power-law in energy $\sim E^{-\alpha}$ up to an energy a factor of 3-10 below the maximum proton energy $E_{\rm p,max}$ where the spectrum breaks due to kinematic limitations in the secondary pion and γ-ray production (Note that we refer to spectra as power laws in energy, with the understanding that this is only asymptotically correct for relativistic energies). At lower energies ($\sim$ 50 MeV to 10 GeV) the spectrum rolls over due to the assumption that the source spectrum is a power-law in momentum and due to the energy dependence of the inclusive cross section for π^0 production, which is strongly energy dependent around the Δ resonance at 1.234GeV (e.g., Stecker 1970; Dermer 1986).

In Fig. 8 the Whipple upper limits and EGRET data are compared with a model for the γ-ray spectrum resulting from secondary π^0-decay. The integral EGRET data points are derived from the differential points in Esposito et al. (1996) for IC443 and γ-Cygni and from the differential spectrum calculated by Fierro (1996) for W44. Also shown are the integral fluxes above 100 MeV from Thompson et al. (1995). Assuming that the $E > 100$ MeV data is dominated by nuclear interactions of cosmic rays, the EGRET spectra and Whipple upper limits are first compared with the γ-ray spectrum calculated from equation 5 for an $E^{-2.1}$ source cosmic-ray spectrum, and normalized to the $E > 100$ MeV integral point. The Whipple upper limits are also compared with a priori model predictions. These model spectra are normalized to the $E > 1$ TeV integral

Table 3. Results of observations.

Object Name	Pointing Direction α(1950)	δ(1950)	Aperture Radius (deg)	ON-Source Counts	OFF-Source Counts	Total Time (min)	Effective Area (10^8cm^2)	Upper Limit (10^{-11}cm^{-2}s^{-1})
Tycho	00^h22^m30	+63°52′23	0.29	315	302	867.2	2.1	0.8
IC443	06 14 00	+22 30 00	0.64	715	654	413.0	1.7	4.2
	06 12 43	+22 19 12	0.64	850	868	663.7	1.6	1.9
	total:		0.64	1565	1522	1076.7		2.1
W44	18 53 29	+01 14 57	0.55	450	426	360.1	1.8	3.0
W51	19 20 00	+14 00 00	0.68	361	294	168.0	1.5	9.6
	19 21 30	+14 00 00	0.68	258	265	300.0	1.7	2.3
	total:		0.68	619	559	468.0		3.6
γ-*Cygni*	20 18 59	+40 15 17	0.76	382	395	252.0	1.6	3.4
	20 20 08	+39 40 36	0.76	319	347	168.0	1.3	5.0
	20 20 00	+40 02 00	0.76	339	362	140.0	1.5	5.6
	total:		0.76	1040	1104	560.0		2.2
W63	20 15 15	+45 24 36	1.05	452	501	140.0	1.3	6.4

flux level given in equation 1 and using the range of values for $\mathscr{A}$ calculated in §2.2. The upper curve assumes a source spectrum of $\propto E^{-2.1}$ and the high value for $\mathscr{A}$ while the lower curve is derived from a soft source spectrum $\propto E^{-2.3}$ and the minimum value for $\mathscr{A}$. Also shown are the upper limits derived from the CASA-MIA and CYGNUS air shower experiments (Borione et al. 1995; Allen et al. 1995) as well as the AIROBICC atmospheric Čerenkov array (Prosch et al. 1996).

6. Discussion

We interpret our results in the context of two hypotheses: (1) that the EGRET data gives evidence for acceleration of cosmic-ray nuclei in SNRs and that the observed γ-ray emission comes not from primary electrons but from nuclear interactions of cosmic rays at their source with ambient material, (2) the EGRET flux is produced by some other mechanism, but a minimum γ-ray flux must be produced in SNRs if they are the sources of cosmic rays and the Whipple upper limits must lie above this predicted flux.

The solid curves in Fig. 8 show an extrapolation from the integral EGRET fluxes assuming an $E^{-2.1}$ source spectrum. In the case of γ-Cygni, IC443 and W44, the Whipple upper limits lie a factor of ∼25, 10 and 10, respectively, below these extrapolations and require either a spectral break or a differential source spectrum steeper than $E^{-2.5}$ for γ-Cygni and $E^{-2.4}$ for IC443. Even the shape of the EGRET spectra, while all having spectral indices near $\alpha \approx 2$, are inconsistent with the shape of the secondary γ-ray spectrum (calculated in §5) for a flat $\sim E^{-2.1}$ cosmic-ray proton spectrum. This suggests a steeper source spectrum and that some additional component such as electron bremsstrahlung is present. This could arise either from primary electrons accelerated at the SNR or from diffuse cosmic-ray electrons interacting with the regions of high density near the SNRs (i.e., an incorrect background model for the EGRET data). Gaisser et al. (1997) perform detailed fits to the multiwavelength data, and have determined that a steep source spectrum $\sim E^{-2.4}$ is required, and that electron bremsstrahlung dominates the low energy emission.

Assuming that an additional bremsstrahlung component would only account for the EGRET emission up to energies of a few hundred MeV (Dermer 1996), if we instead extrapolate from the EGRET data at energies above 1 GeV, the disagreement with the Whipple upper limits is reduced to a factor of ≈7, 3 and 5 below the extrapolation for γ-Cygni, IC443 and W44, respectively. In any case, if the EGRET data have an appreciable contribution from π^0-decay then the Whipple results and the EGRET spectra require either a steep source spectrum or a spectrum which cuts off below 10 TeV, in contradiction to expectations for the γ-ray emission from a typical source of cosmic rays.

An alternative explanation of the >100 MeV emission is that the observed γ-rays are dominated by emission from high energy electrons accelerated either in the vicinity of pulsars or in the SNR shocks. Brazier et al. (1996), De Jager & Mastichiadis (1997) and Harrus et al. (1996) provide evidence in support of the pulsar hypothesis for 2EG 2020+4026 and 2EG 1857+0118. The observation of nonthermal X-rays in the limbs of IC443 by Keohane et al. (1997) provides evidence for high energy electrons produced by shock acceleration. But even if the EGRET results do not provide direct evidence for γ-rays from nuclear interactions, an additional γ-ray flux from cosmic rays accelerated in the shocks of these SNRs is still expected.

Also shown in Fig. 8 are the predictions of the γ-ray flux derived from equation 1 and given our best estimates of the SNR parameters (see §2.2), assuming a range of spectral indices between 2.1 and 2.3 at the source. Using a conservative value for the average value density of the interstellar medium ~ 0.1 cm^{-3} and the canonical supernova explosion energy of $\sim 10^{51}$ ergs yields a flux prediction for each SNR which is not inconsistent with the Whipple upper limits. However, IC443, γ-Cygni and W44 have been selected because of the strong evidence for an association with a nearby molecular cloud which would greatly enhance the local ISM density and hence the predicted γ-ray flux (see equation 1). For IC443 in particular, the higher flux

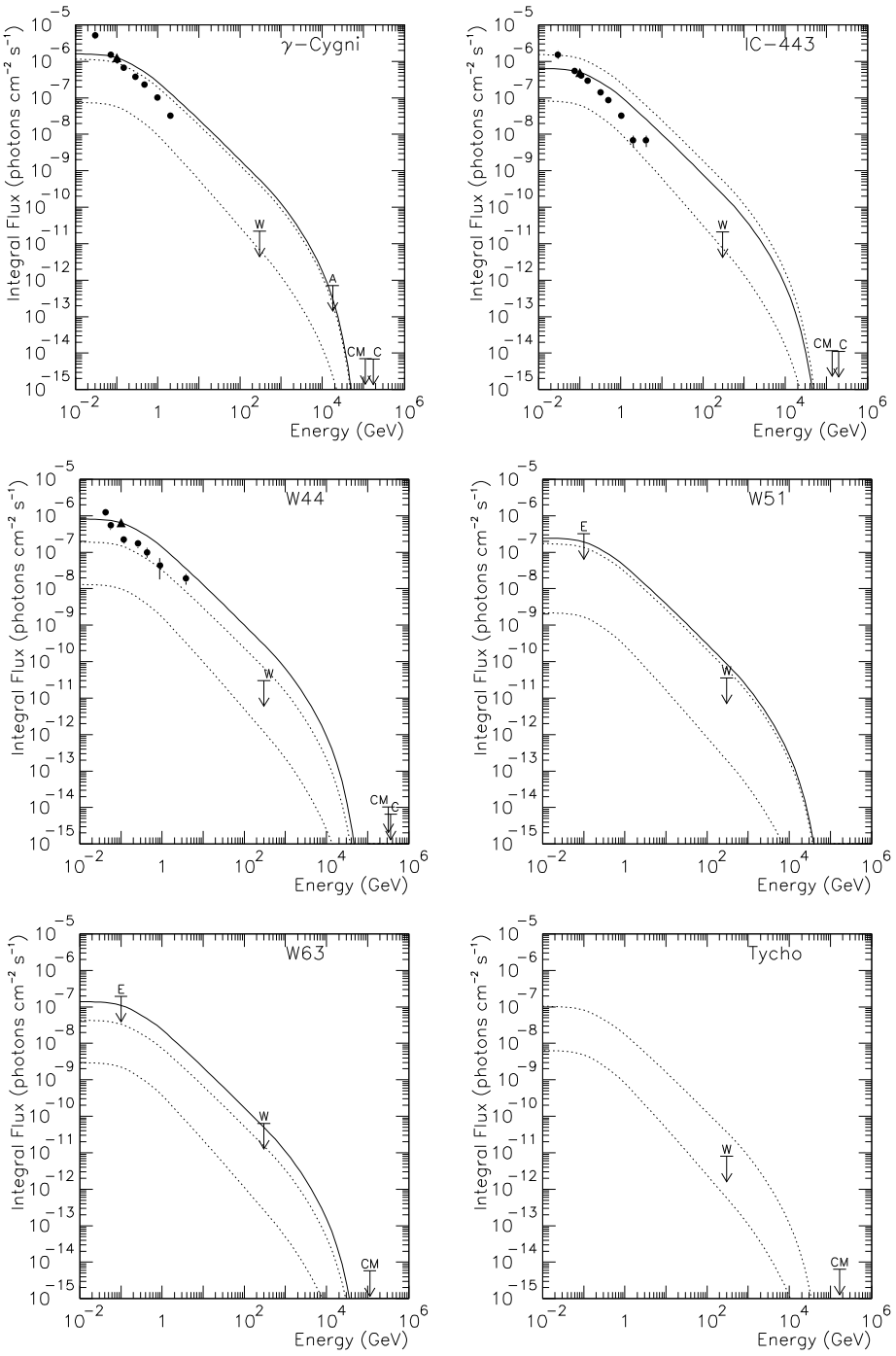

Fig. 8. Whipple upper limits (W) shown along with EGRET integral fluxes (filled triangles), integral spectra (filled circles) and approximate flux upper limits from Esposito et al. (1996) (E). These are compared to extrapolations from the EGRET integral data points (solid curves), as well as a conservative estimate of the allowable range of fluxes from the model of Drury et al. (1994) (dashed curves). Also shown are CASA-MIA upper limits (CM) from Borione et al. (1995), CYGNUS upper limits (C) from Allen et al. (1995), and the AIROBICC upper limit (A) from Prosch et al. (1996)

prediction is also the most realistic. Furthermore, our procedure for calculating the upper limits whereby we consider emission from the whole remnant is quite conservative. When we restrict our aperture to the region of the molecular clouds in γ-Cygni and IC443 where the bulk of the γ-ray emission is expected to be produced, the upper limits are significantly reduced, but uncertainties in the matter distribution make these limits difficult to interpret.

In general we expect that roughly one half of the Galactic SNRs result from the core-collapse of young massive stars which explode into star formation regions or regions which are disturbed by mass-loss of the progenitor (e.g., Drury 1995; Huang & Thaddeus 1986). Montmerle (1979) and others have provided evidence for this connection through observations of spatial coincidences between SNRs and OB associations. Large molecular clouds are the birth-places for OB associations, and Huang & Thaddeus (1986) found in a CO survey toward 26 SNR, that roughly half of them revealed spatial coincidences with large molecular cloud complexes. Since the enhanced γ-ray signal resulting from a dense molecular cloud should be

easily detectable, even in the absence of the EGRET results the non-detections of 300 GeV emission for all six SNRs is surprising, and is beginning to provide serious constraints on the allowed parameter space for SNR models for the origin of cosmic rays.

Baring, Ellison & Grenier (1997) have emphasized that for young SNRs, age/size limits to the acceleration may result in low energy cutoffs in the γ-ray spectrum which could potentially account for the upper limits at TeV and higher energies. Following DMV, the maximum energy for diffusive shock acceleration is obtained by integrating the equation $dp_{\rm max}/dt = p_{\rm max}/\tau_{\rm acc}(p_{\rm max})$, where the acceleration timescale $\tau_{\rm acc}$ depends on the shock compression ratio r, the diffusion coefficient κ and the shock velocity $\dot{R}_{\rm S}$:

$$\tau_{\rm acc} \propto \frac{r(r+1)}{(r-1)} \frac{\kappa(p)}{\dot{R}_{\rm S}^2}. \quad (5)$$

In the Bohm limit the diffusion constant is given by $\kappa \approx r_g c/3$, where $r_g = cp/ZeB$ is the gyroradius for a particle of momentum p. Integrating equation 5 in the initial free expansion phase ($R_{\rm S} \propto t$), the maximum proton energy grows linearly with time according to:

$$\left(\frac{E_{\rm max}}{100\ {\rm TeV}}\right) = Z \left(\frac{B}{5\ \mu{\rm G}}\right) \left(\frac{t_{\rm SNR}}{10^4\ {\rm yr}}\right) \left(\frac{\dot{R}_{\rm S}}{2000\ {\rm km/s}}\right)^2 \quad (6)$$

The condition that the diffusion scale not exceed the dimension of the SNR, $\kappa/\dot{R}_{\rm S} < R_{\rm S}$, gives a similar limit (Baring, Ellison & Grenier 1997). Once the SNR enters its adiabatic expansion phase, $R_{\rm S} \propto t^{2/5}$ and the maximum proton energy increases very slowly (DMV). In this case, equation 6 using the present (decelerated) value for the shock speed $\dot{R}_{\rm S}$ (300-1000 km/sec for IC443, γ-Cygni W44 and W51; Lozinskaya 1992) gives a lower limit on $E_{\rm max}$. Detailed calculations by DMV and DAV show that the maximum energy and maximum luminosity are reached in a few thousand years for typical ISM densities, or less for SNRs expanding into a dense medium. Even for Tycho, the youngest remnant we have observed with an age of $t_{\rm SNR}$ = 435 yr and $\dot{R}_{\rm S} > 2000$ km/s (Smith et al. 1988), equation 6 gives $E_{\rm max} > 4$ TeV, resulting in a roll-over in the γ-ray spectrum at energies between 400 GeV and 1 TeV (see §5). If the other older SNRs considered here are typical of remnants in their Sedov phase then the maximum cosmic-ray energy $\sim$100 TeV should have been obtained.

One might try to explain the discrepancy by arguing that these remnants were poorly selected, and are not representative of the type of SNR which provide the sites for cosmic-ray acceleration. For example they have very low shock velocities (Baring et al. 1997) or perhaps low magnetic fields. It is also possible that the higher ambient density from the associated molecular clouds may have either stopped the acceleration early or has resulted in damping of the scattering waves thereby quenching the acceleration (Drury et al. 1996). But the efficiency of 10-30% derived from the cosmic-ray power budget assumes that *all* SNR are cosmic ray sources. If the observations reduce the fraction of objects for which the process is viable, then the efficiency requirements are increased, possibly to uncomfortable levels, for the remaining objects.

A final caveat is that the source spectrum and cosmic-ray energy budget inferred from propagation models could be in error because of some oversimplification in these models. Other possibilities for cosmic-ray transport such as the nested leaky box model (e.g., Cowsik & Wilson 1973) or the reacceleration scenario of Seo & Ptuskin (1994) imply a steeper source spectrum with $\alpha \approx 2.3 - 2.7$ without violating the observed energy dependence of the secondary to primary ratio (see Gaisser 1990 for a review of propagation models). The reacceleration model involves a simple modification of the cosmic-ray transport equation based on the natural assumptions that the scattering on hydromagnetic waves causes both a spatial and energy diffusion of the cosmic-ray particles, and that the interstellar turbulence has a Kolmogorov spectrum (Seo and Ptuskin 1994). However, a flat power-law spectrum $\sim E^{-2}$ has been advocated as a robust feature of diffusive shock acceleration models, and some significant modification of the acceleration theory would be, for the first time, required by the data.

7. Conclusion

Data taken with the Whipple Observatory γ-ray telescope on a number of radio-bright SNRs have been used to test the model of cosmic-ray acceleration in the blast shocks of supernova remnants. The model predictions for the γ-ray luminosity of SNRs are strongly tied to cosmic-ray data as well as to the observational data on individual SNRs. While the suggestion has been made that the association of unidentified EGRET sources with SNRs provides evidence that SNRs are the sites for cosmic ray acceleration, when combined with the EGRET data, the Whipple upper limits are inconsistent with the model extrapolation, indicating a steep spectrum or perhaps a spectral cutoff for IC443, γ-Cygni and W44. While the EGRET integral fluxes are approximately consistent with the model predictions, the shape of the EGRET spectra are inconsistent with that expected to arise from nuclear interactions from a flat cosmic-ray source spectrum.

The Whipple upper limits are measured at 300 GeV, well below the energy at which one might expect a cutoff in the γ-ray spectrum either from direct measurements of cosmic-ray spectra or from shock acceleration theory. Taken alone, the Whipple results strongly constrain model predictions for a number of sources and are inconsistent with the predictions for emission from these SNRs if dense molecular clouds are in fact present and if the efficiency for conversion of the kinetic energy of the supernova explosion is $\sim$10$-$30% as derived from the cosmic-ray power budget.

Acknowledgements. We would like to thank Patrick Boyle, Javier Bussóns Gordo, Kevin Harris, Teresa Lappin and Frank Samuelson for assistance in obtaining these data. We would also like to thank Chuck Dermer and Peter Duffy for valuable discussions and suggestions as well as Steve Sturner for assistance with calculations of the γ-ray spectra. This research was supported by the U.S. Department of

Energy, by NASA grants from CGRO, by PPARC in the U.K. and by Forbairt in Ireland.

References

Aharonian, F.A., Drury, L.O'C., Völk, H.J., 1995, A&A 150, 339
Akerlof, C.W., et al., 1991, ApJ 377, L97
Allen, G.E., et al., 1995, ApJ 448, L25.
Angerhofer, P.E., Becker, R.H., Kundo, M.R., 1977, A&A 55, 11
Axford, W.I., Leer, E., Skadron, G., 1977, in Proc. of the 15th ICRC (Budapest), vol. 7, p. 132
Baring, M.G., Ellison, D.C., Grenier, I., 1997, in Proc. of the 2nd Integral Workshop (St. Malo), in press
Bell, A.R., 1978, MNRAS 182, 147
Bertsch, D.L., Dame, T.M., Fichtel, C.E., et al., 1993, ApJ 416, 587
Blandford, R.D., Ostriker, J.P., 1978, ApJ 221, L29
Blandford, R.D., Ostriker, J.P., 1980, ApJ 237, 793
Borione, A., Catanese, M., Covault, C.E. et al. 1995, in Proc. of the 24th ICRC (Rome), vol. 2, p. 439
Braun, R., Strom, R.G. 1986, Astr. Ap. 164, 193
Brazier, et al., 1996, MNRAS 281, 1033
Buckley, J., Dwyer, J., Müller, D., et al., 1994, ApJ 429, 736
Buckley, J.H., Boyle, P.J., Bradbury, S.M., et al., 1997, in Proc. of the 25th ICRC, in press
Burton, W.B., & Shane, W.W. 1970, in IAU Symposium No. 83, The Spiral Structure of Our Galaxy, ed. W. Becker, G. Contopoulos (Dordrecht; Reidel), p. 397
Catanese, M., Akerlof, C.W., Biller, S. 1995, in Proc. of the Workshop: Towards a Major Atmospheric Cherenkov Detector-IV, ed. M. Cresti, Padova, p. 335
Cawley, M.F., et al., 1990, Exper. Astr. 1, 173
Chevalier, R.A., Kirshner, R.P., Raymon, R.C., 1980, ApJ 235, 186
Clark, D.H., Green, A.J. & Caswell, J.L. 1975, Aust. J. Phys. Astrphys. Suppl. 37, 75
Condon, J.J., et al., 1994, AJ 107, 1829
Cong, H.I., 1977, Ph.D. Dissertation, Columbia University
Connaughton, V., 1996, Ph.D. Thesis, University College Dublin
Cornett, R.H., Chin, G., Knapp, G.R., 1977, A. Ap. 54, 889
Cowsik, R.& Wilson, L. 1973, in Proc. 13th ICRC (Denver) vol. 1, p. 500
Dame, T.M., Ungerechts, H., Cohen, R.S., et al., 1987, ApJ 322, 706
De Jager, O.C. & Mastichiadis, A. 1997, ApJ, in press
DeNoyer, L.K., 1979, ApJ 228, L41
DeNoyer, L.K., 1979, ApJ 232, L165
DeNoyer, L.K., 1983, ApJ 264, 141
DeNoyer, L.K., Frerking, M.A., 1981, ApJ 246, L37
Dermer, C.D., 1986, A&A 157, 223
Dermer, C.D., 1996, private communication
Drury, L. O'C., Markiewicz, W.J., Völk, H.J., 1989, A&A 225, 179
Drury, L. O'C, Aharonian, F.A., Völk, H.J., 1994, A&A 287, 959
Drury, L. O'C., 1995, in Towards a Major Atmospheric Čerenkov Detector-IV, ed. M. Cresti, (University of Padova; Padova), p. 76
Drury, L. O'C., Duffy, P., Kirk, J., 1996, A&A 309, 1002
Ellison, D.C., Reynolds, S.P., 1991, ApJ 382, 242
Engelmann, J.J., Ferrando, P., Soutoul, A., et al., 1990, A&A 233, 96
Erickson, W.C., Mahoney, M.J., 1985, ApJ 290, 596
Esposito, J.A., Hunter, S.D., Kanbach, G., Sreekumar, P., 1996, ApJ 461, 820
Fesen, R.A., 1984, ApJ 281, 658
Fierro, J., 1996, Ph. D. Dissertation, Stanford University
Fukui, Y., Tatematsu, K., 1988, in IAU Colloquium 101: Supernova Remnants and the Interstellar Medium, eds. R.S. Roger, T.L. Landecker, Cambridge University Press, Cambridge, p. 261
Fürst, E. et al. 1990, A&A Suppl. Ser., 85, 691.
Gaisser, T.K., 1990, Cosmic Rays and Particle Physics, Cambridge University Press, Cambridge
Gaisser, T.K., Protheroe, R.J., Stanev, T., 1997, ApJ, submitted
Green, D.A., 1984, MNRAS 209, 449
Green, D.A., 1986, MNRAS 221, 473
Green D.A., 1989, MNRAS 238, 737
Green, D.A., 1995, A Catalog of Galactic Supernova Remnants (1995 July version), Mullard Radio Astronomy Observatory, Cambridge, United Kingdom (available on the World-Wide-Web at "http://www.mrao.cam.ac.uk/surveys/snrs/")
Hamilton, A.J.S., Sarazin, C.L., Szymkowiak, A.E., 1986, ApJ 300, 713
Harrus, I.M., Hughes, J.P., Helpand, D.J., 1996, ApJ 464, L161
Heavens, A.F., 1984, 211, 195
Helene, O., 1983, NIM 212, 319
Higgs, L.A., Landecker, T.L., Roger, R.S., 1977, AJ 82, 9
Higgs, L.A., Landecker, T.L., Seward, F.D., 1983, in Supernova and their X-Ray Emission, eds. J. Danziger & P. Gorenstein, (IAU) p. 281
Higgs, L.A., et al., 1991, J. R. Astron. Soc. Can. 85, 24
Huang, Y.-L., Thaddeus, P., 1986, ApJ 309, 804
Hunter, S.D., Bertsch, D.L., Catelli, J.R., et al., 1997, ApJ 481, 205
Kamper, & van den Bergh, 1978, ApJ 224, 851
Keohane, J.W., Petre, R., Gotthelf, E.V., et al., 1997, ApJ, in press
Koo, B.-C., Kim, K.-T., Seward, F.K., 1995, ApJ 447, 211
Koo, B.-C., Moon, D.-S., 1997, ApJ 475, 194
Koyama, M., Petre, R., Gottheif, E.V., et al., 1995, Nature 378, 255
Krymsky, G.F., 1977, Dokl. Akad. Nauk SSSR, 234, 1306 (Engl. transl. Sov. Phys.-Dokl., 23, 327)
van der Laan, H., 1962, MNRAS 124, 125
Landecker, T.L., Roger, R.S., Higgs, L.A., 1980, A&AS 39, 133
Lang, M., 1991, Ph.D. thesis, National University of Ireland
Legage, P.O. & Cesarsky, C.J. 1983, A&A, 118, 223
Lessard, R.W., Akerlof, C.W., Biller, S.D., et al., 1995, in: Proc. 24th ICRC (Rome), vol. 2, p. 475
Lessard, R.W., 1997, Ph.D. thesis, National University of Ireland
Lessard, R.W., Buckley, J.H., & Connaughton, V. 1997, in preparation
Li, T.-P., Ma, Y.-Q., 1983, ApJ 272, 317
Lozinskaya, T.A., 1992, Supernova and Stellar Wind in the Interstellar Medium, (New York; AIP)
Montmere, T., 1979, ApJ 231, 95
Mastichiadis, A., 1996, A&A, 305, 53
Müller, D., Swordy, S.P., Meyer, P., L'Heureux, J., Grunsfeld, J.M., 1991, ApJ 374, 356
Mattox, J.R., Bertsch, D.L., Chiang, J., et al., 1996, ApJ 461, 396
Mohanty, G., et al., 1997, in preparation
Moon, D.-S., Koo, B.-C., 1994, Journal of the Korean Astron. Soc. 27, 81
Naito, T., Takahara, F., 1994, J. Phys. G: Nucl. Part. Phys. 20, 477
Petre, R., Szymkowiak, A.E., Seward, F.D., Willingale, R., 1988, ApJ 335, 215
Pollock, A.M.T., 1985, A&A 150, 339
Prosch, C., Feigl, E., Plaga, R., et al., 1996, A&A 314, 275
Punch, M., Akerlof, C.W., Cawley, M.F., et al., 1991, in Proc. 22nd ICRC (Dublin), vol. 1, p. 464
Punch, M., 1993, Ph.D. thesis, National University of Ireland
Reynolds, S.P., Ellison, D.C., 1992, ApJ 399, L75

Reynolds, P.T., Akerlof, C.W., Cawley, M.F., 1993, ApJ 404, 206
Reynolds, S.P., 1995, Nature 378, 232
Reynolds, S.P., 1996, ApJ 459, L13
Rho, J.-H., Petre, R., Schlegel, E.M., 1994, ApJ 430, 757
Rho, J.-H., 1995, Ph.D. Dissertation, University of Maryland
Rosado, M. & Gonzalez, J. 1981, Mex. Astron. Astrof., 5, 93
Sato, F., 1974, AJ 91, 378
Scoville, N.Z., Irvine, W.M., Wannier, P.G., Predmore, C.R., 1977, ApJ 216, 320
Seo, E.S., Ptuskin, V.S., 1994, ApJ 431, 705
Seward, F.D., 1990, ApJS 73, 781
Seward, F.D., Gorenstein, P., Tucker, W., 1983, ApJ 266, 287
Seward, F.D., Kearns, Rhode, 1997, ApJ, in press
Smith, A., Davelaar, Peacock, A., Taylor, B.G., Morini, M., Robba, N.R., 1988, ApJ 325, 288
Sreekumar, P., et al., 1993, Phys. Rev. Let. 70, 127
Stecker, F.W., 1970, Astro. Space Sci. 6, 377
Stephens, S.A., Badhwar, G.D., Astro. Space Sci. 76, 213
Strom, R.G., Goss, W.M., Shaver, P.A., 1982, MNRAS 200, 473
Sturner, J.A., Dermer, C.D., 1994, A&A 293, L17
Sturner, S.J., Skibo, J.G., Dermer, C.D., 1997, in preparation
Swordy, S.P., Müller, D., Meyer, P., L'Heureux, J., Grunsfeld, J.M., 1990, ApJ 349, 625
Tan, S.M., Gull, S.F., 1985, MNRAS 216, 949
Thompson, D.J., Bertsch, D.L., Dingus, B.L., et al., 1995, ApJS 101, 259
Toor, A., Seward, F., 1977, ApJ 216, 560
Treffers, R.R., 1979, ApJ 233, 17
Vacanti, G., et al., 1991, ApJ 377, 467
Velusamy, T., Kundu, M.R., 1974, A&A 32, 375
Völk, H.J., 1987, in Proc. 20th ICRC (Moscow), vol. 7, p. 157
Völk, H.J., Biermann, P.L., 1988, ApJ 333, L65
Wendker, H.J., 1971, A&A 13, 65
Wolszczan, et al., 1991, ApJ 372, L99
Wootten, H.A., 1977, ApJ 216, 440

This article was processed by the author using Springer-Verlag LaTeX A&A style file *L-AA* version 3.